Macro-and Microstructural, Textural Fabrics and Deformation Mechanism of Calcite Mylonites from Xar Moron-Changchun Dextral Shear Zone, Northeast China

LIANG Chenyue[1, 2*], LIU Yongjiang[3, 4*], ZHENG Changqing[1, 2], LI Weimin[1, 2], Franz NEUBAUER[5] and ZHANG Qian[1]

[1] *College of Earth Sciences, Jilin University, Changchun, Jilin, 130061, China*
[2] *Key laboratory of Mineral Resources Evaluation in Northeast Asia, Ministry of Land and Resources, Jilin University, Changchun, Jilin, 130061, China*
[3] *Key Lab of Submarine Geosciences and Prospecting Techniques, Ministry of Education, College of Marine Geosciences, Ocean University of China, Qingdao, Shandong, 266100, China*
[4] *Laboratory for Marine Mineral Resources, Qingdao National Laboratory for Marine Science and Technology, Qingdao, Shandong, 266237, China*
[5] *Department of Geography and Geology, University of Salzburg, Salzburg, A-5020, Austria*

Abstract: The calcite mylonites in the Xar Moron-Changchun shear zone show a significance dextral shearing characteristics. The asymmetric (σ-structure) calcite/quartz grains or aggregates, asymmetry of calcite c-axes fabric diagrams and the oblique foliation of recrystallized calcite grains correspond to a top-to-E shearing. Mineral deformation behaviors, twin morphology, C-axis EBSD fabrics, and quartz grain size-frequency diagrams demonstrate that the ductile shear zone was developed under conditions of greenschist facies, with the range of deformation temperatures from 200 to 300 °C. These subgrains of host grains and surrounding recrystallized grains, strong undulose extinction, and slightly curved grain boundaries are probably results of intracrystalline deformation and dynamic recrystallization implying that the deformation took place within the dislocation-creep regime at shallow crustal levels. The calculated paleo-strain rates are between $10^{-7.87}$ s^{-1} and $10^{-11.49}$ s^{-1} with differential stresses of 32.63–63.94 MPa lying at the higher bound of typical strain rates in shear zones at crustal levels, and may indicating a relatively rapid deformation. The S-L-calcite tectonites have undergone a component of uplift which led to subhorizontal lifting in an already non-coaxial compressional deformation regime with a bulk pure shear-dominated general shear. This E-W large-scale dextral strike-slip movement is a consequence of the eastward extrusion of the Xing'an-Mongolian Orogenic Belt, and results from far-field forces associated with Late Triassic convergence domains after the final closure of the Paleo-Asian Ocean.

Keywords: Calcite mylonites, EBSD analysis, Finite-strain determination, Kinematic vorticity, Paleopiezometry, Solonker-Xar Moron-Changchun-Yanji Suture Belt

E-mail: chenyueliang@jlu.edu.cn (C. Y. Liang), liuyongjiang@ouc.edu.cn (Y. J. Liu)

1 Introduction

Shear zones are narrow, planar and places where the strain is locally concentrated relative to their surrounding regions (Ramsay, 1980; Means, 1995; Holyoke and Tullis, 2006). Structural geologists have long been interested in ductile shear zones (e.g., Simpson and De Paor, 1993; Xypolias and Doutsos, 2001; Tikoff and Greene, 1997; Bahattacharya and Weber, 2004; Yang, 2005; Zhu et al., 2006; Liang et al., 2015; Zhang et al., 2014, 2017; Cao et al., 2011, 2017). Mylonitic rocks in ductile shear zones are products of ductile deformation in the middle to lower crust, and their fabric evolution is closely related to strain intensities, shear types, rheological parameters as well as meso- and micro-structures (Lister, 1977; Sibson, 1977; Brodie, 1980; Wernicke, 1985; Zheng, 1999; Wang et al., 2002, 2007; Li et al., 2010; Wang et al., 2011; Liu et al., 2012; Liang et al., 2015; Zhang et al., 2014, 2017; Cao et al., 2011, 2017), which are commonly characterized by dynamic recrystallization and grain size reducing (Zheng and Chang, 1985; Tikoff and Fossen, 1995, 1999; Zheng and Wang, 2005).

Carbonatites are mainly composed of calcite ($CaCO_3$), variable amounts of dolomite ($CaMg(CO_3)_2$) and minor ankerite ($CaFe(CO_3)_2$). These most abundant minerals present in the middle and upper crust found in shear zones which likely control the rheology of these zones (Heard and Raleigh, 1972; Rutter, 1972, 1974; Schmid et al., 1977; Schmid et al., 1980; Walker et al., 1990; De Bresser, 2001; Renner et al.,

2002; Herwegh et al., 2005; Austin and Evans, 2009; Liang et al., 2015; Zhang et al., 2017; Cao et al., 2017). Macro-microfabric studies in low grade carbonate mylonites provide crucial data on deformation conditions and kinematics from upper crust (Burkhard, 1993; Leiss et al., 1999; De Bresser, 2001; Bestmann et al., 2000, 2006; Llana-Fúnez and Rutter, 2008; Marques et al., 2015; Liang et al., 2017). Compared to other common shallow crustal minerals like quartz (plastic flow not below 270 °C; e.g. Voll, 1976; Stipp et al., 2010) and feldspar (above 450–500 °C; Bell and Johnson, 1989; Kruse et al., 2001), crystal plastic slip in calcite starts at a lower temperature (about 180 °C), and can accumulate large amounts of strain with progressive deformation or increasing of pressure-temperature (e.g., Rutter, 1974, 1995; Schmid et al., 1977, 1980, 1987; Wenk et al., 1987; Walker et al., 1990; Rutter et al., 1994; Bestmann et al., 2000; De Bresser, 2002; Renner et al., 2002; Llana-Fúnez and Rutter, 2008). The calcite has important consequences for understanding the rheology of the upper lithosphere, thermal history, tectonic evolution, kinematics and related deformation-metamorphic processes (Poirier, 1980; Rutter and Brodie, 1988; Van der Pluijm, 1991; Busch and Van der Pluijm, 1995; Montési and Hirth, 2003; Bestmann and Prior, 2003; Bestmann et al., 2000, 2006; Negrini et al., 2018).

Central-Eastern Asia, located between the North China Craton (NCC) and Tarim Craton in the south and the Siberian Craton in the north, recorded the Neoproterozoic to Paleozoic evolution of the Central Asian Orogenic Belt (CAOB; e.g. Sengör et al., 1993; Xiao et al., 2003; Jahn, 2004; Xu et al., 2013; Liu et al., 2017; Zhou et al., 2018; Dai et al., 2018; Yu et al., 2018, 2019a, b; Fig. 1). It was traditionally believed by many studies that the Solonker-Xar Moron-Changchun-Yanji Suture Belt (Fig. 1 and 2a) marks the site of the final closure of the Paleo-Asian Ocean and this suture has become the focus of many recent studies (Enkin et al., 1992; Xiao et al., 2003; Jia et al., 2004; Sun et al., 2004; Li, 2006; Wu et al., 2007, 2011; Cao et al., 2013; Sun et al., 2013; Xu et al., 2013; Zhou and Wilde, 2013; Eizenhöfer et al., 2014; Safonova and Santosh, 2014; Han et al., 2016; Han et al., 2017; Wang et al., 2015, 2016; Wilde, 2015; Du et al., 2017; Liu et al., 2017). Many studies surrounded the Paleo-Asian Ocean have been carried out during the past decades in order to identify the geological characteristics, isotopic ages, ore genesis, origin and evolution of the associated intrusions as well as the corresponding geodynamic settings (Chen et al., 2008; Liu et al., 2010; Ma et al., 2013; Sun et al., 2013; Zhang et al., 2009a, b, 2010, 2012; Zhou et al., 2018).

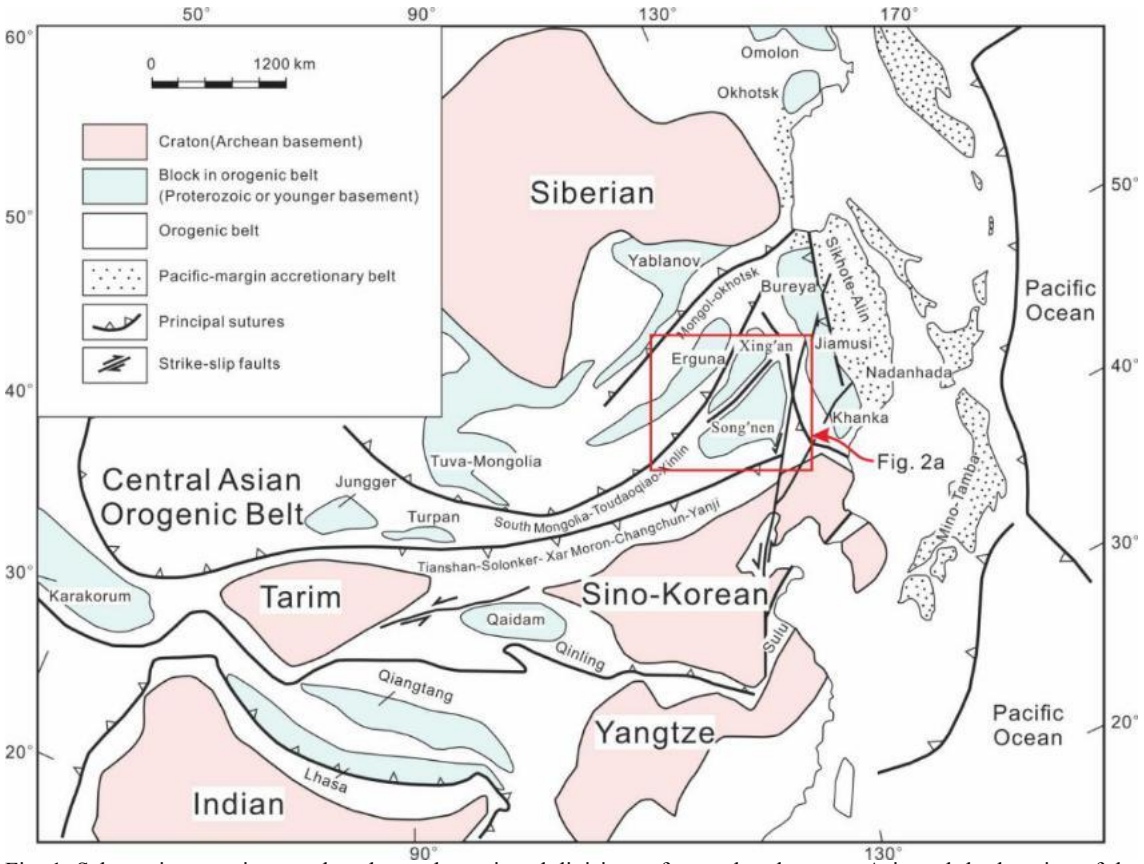

Fig. 1. Schematic tectonic map that shows the main subdivisions of central and eastern Asia and the location of the study area (modified from Zhou et al., 2018).

The Early Mesozoic evolution along the Solonker-Xar Moron-Changchun-Yanji Suture Belt is also not well understood, which is a crucial period in deciphering the tectonic transition from Paleozoic evolution

of the CAOB to the Late Mesozoic (Meng, 2003; Li, 2006; Li et al., 2014). Several Early Mesozoic strike-slip faults on the northern margin of the NCC were described preliminarily, e.g., the western Xar Moron-Changchun Fault or ductile shear zone, activated along the Solonker-Xar Moron-Changchun-Yanji Suture Belt (Zhao et al., 2015), and Chicheng-Fengning-Longhua Fault (Wang et al., 2013), which give us good opportunities to study the Early Mesozoic kinematics and deformation in this area. There has been also a special outpouring of concern for the reactivation and deformation along the Xar Moron-Changchun Fault, as the suture belt of the final closure of the Paleo-Asian Ocean. It can give important clues to decipher the Early Mesozoic tectonic evolution of the northern margin of NCC, eastern of CAOB or southern of Xing'an-Mongolian Orogenic Belt (XMOB) which consists of Erguna, Xing'an Songnen, Jiamusi and Khanka massifs and several orogenic belts between them (Xu et al., 2013, 2015; Liu et al., 2017; Zhou et al., 2018).

In the central part of Xar Moron-Changchun Fault (south of Changchun) exposed lots of Carboniferous carbonatites (C_3s Shizuizi Formation, C_2m Mopanshan Formation and C_1l Luquantun Formation), which are strongly deformed and show a significance dextral shearing characteristics. These exposures of this shear zone present an excellent opportunity to perform multidisciplinary investigation on the effects of calcite on the rheological, microstructural, structural features during dextral shearing in Carboniferous to Mesozoic. Hence, this study presents a multi-disciplinary macro-microstructural, textural electron backscatter diffraction (EBSD), geometry, paleopiezomety analysis of a shear zone in calcite mylonites located in the south of Changchun. We named it as the Xar Moron-Changchun dextral shear zone (eastern part of Xar Moron-Changchun Fault; Fig. 1 and 2), and we try to discuss its place in the Early Mesozoic tectonic framework of eastern CAOB, but also provide further insights into the Permian-Triassic tectonic evolution of the eastern segment of the Paleo-Asian Ocean.

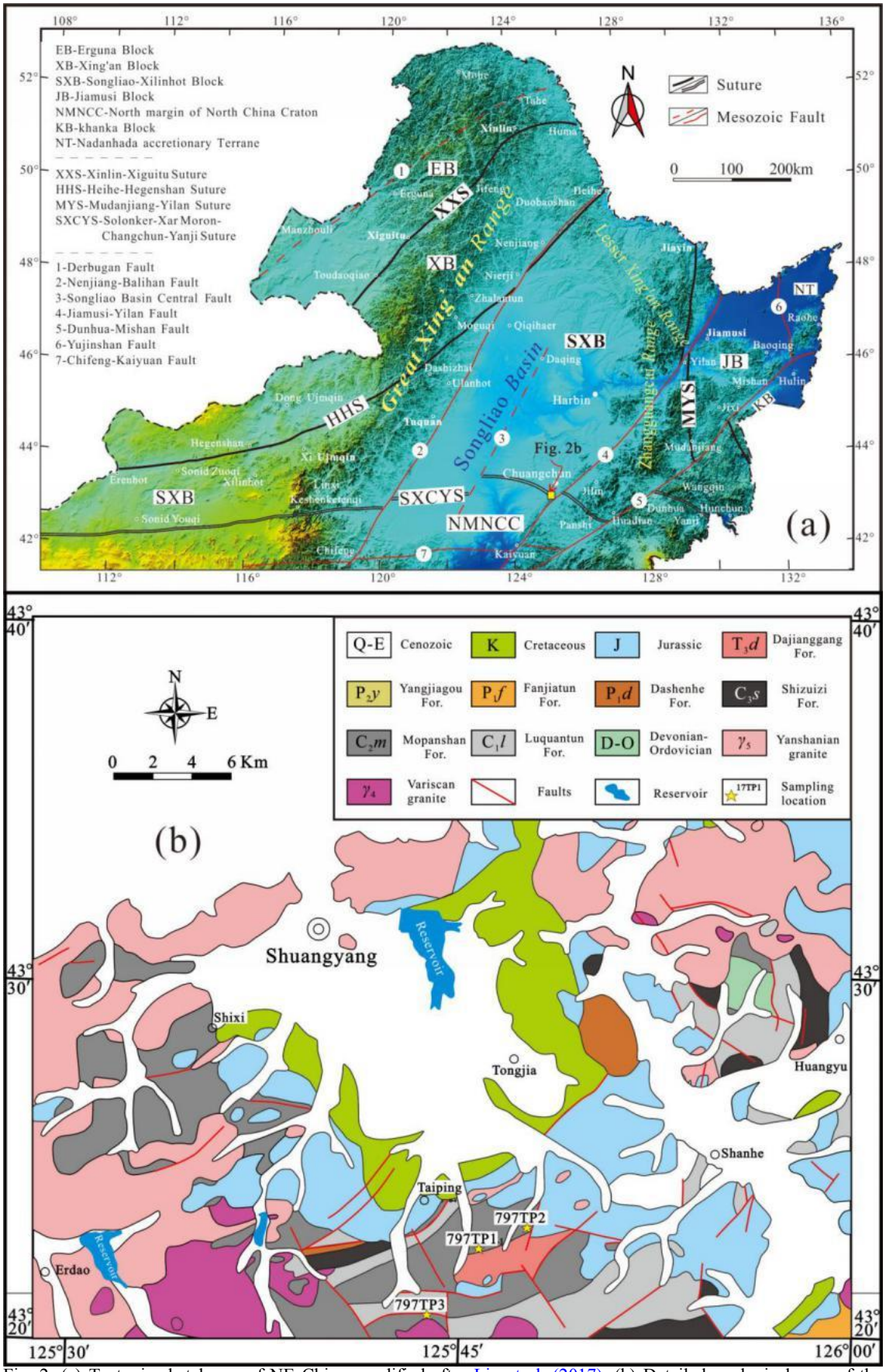

Fig. 2. (a) Tectonic sketchmap of NE China, modified after Liu et al. (2017). (b) Detailed geological map of the Changchun-Shuangyang area in central Jilin Province with sampling locations.

2 Geological Setting

The Central Asian Orogenic Belt (CAOB; Fig. 1) is one of the largest and most complex orogenic collages in the world, which preserves crucial evidence for Phanerozoic juvenile crustal growth (Sengör et al., 1993; Wilde et al., 2000, 2003; Jahn, 2004; Xiao et al., 2003, 2015; Kröner et al., 2014, 2017; Windley et al., 2007; Safonova et al., 2011; Safonova and Santosh, 2014; Xiao and Santosh, 2014; Wilde, 2015; Wilde and Zhou, 2015; Cai et al., 2016; Liu et al., 2017; Safonova, 2017). This huge Phanerozoic suture belt is regarded as a natural laboratory for exploring the geodynamic processes during accretionary orogenesis and continental growth (Xiao and Santosh, 2014). During its long tectonic evolutionary history, the Northeast China or Xingan'an Mongolian Orogenic Belt (XMOB) witnessed the evolution and final closure of the Paleo-Asian Ocean and the amalgamation of micro-continental blocks, which from southeast to northwest are the Jiamusi-Khanka, Songliao-Xilinhot, Xing'an, and Erguna blocks (Fig. 2a; Wu et al., 2007, 2011; Cao et al., 2013; Wilde, 2015; Liu et al., 2017; Zhou et al., 2018). This region also witnessed overprinting by the circum-Pacific tectonic domain in the east and the Mongol-Okhotsk tectonic domain in the northwest during the Mesozoic (Li, 2006; Windley et al., 2007; Wu et al., 2007; Xu et al., 2009a; Zhou and Wilde, 2013; Guo et al., 2015; Wilde, 2015; Wilde and Zhou, 2015; Li et al., 2019; Liang et al., 2019).

The Xar Moron-Changchun Fault as the suture belt of the final closure of the Paleo-Asian Ocean, which is documented by both geological (Li, 2006) and geophysical evidence (Liu et al., 2008; Chen et al., 2008). Most of the eastern Xar Moron-Changchun Fault is hidden by desert sands and Cenozoic sediments, notably, the central segment has well-exposed mylonites (Figs.1 and 2a), and is chosen as the target for this study (Fig. 2b and 3a).

In the south of Changchun, Taiping Town, exhibits a pervasive ductile deformation. From a litho-stratigraphic point of view, this location exposes the following succession in an ascending order (IMBGMR, 1991). The Ordovician-Devonian (O-D) is mainly composed of schist, limestone, slate, sandstone, and volcanic-sedimentary rocks. The Carboniferous sequence is deformed limestone, with dextral shearing fabrics showing obvious E-W striking foliations and sub-horizontal lineation (Fig. 3b). A weak and local metamorphic Permian volcanic-sedimentary sequence overlies the Early Paleozoic calcite mylonites (Fig. 2b and 3c). In the Mesozoic, the whole area came into a terrestrial environment, and deposition was absent except for the Late Triassic-Jurassic continental volcanic-sedimentary deposits (IMBGMR, 1991). Lastly, undeformed Early Cretaceous granites intruded into older rocks, and terrestrial sedimentary rocks overlaid (Fig. 2b).

The shear zone boundaries are parallel to the main foliation of the coarse-grained calcite mylonites. Rare mica flakes in the coarse grained mylonites define a mineral lineation. For the detailed laboratory and microscopic studies, we collected oriented calcite mylonite samples from Early Carboniferous C_1l Luquantun Formation in quarries where the shear zone is well exposed (Fig. 3a). Crystallographic and shape fabrics describe preferred orientations with respect to a fixed sample reference system. Conventionally the main foliation is used as the reference plane. The main foliation is usually parallel to the direction of shearing. In this study, the axes of the sample reference frame are defined by *X* parallel to the mineral lineation, *Z* normal to the shear zone boundary, and *Y* perpendicular to both. Polished thin-sections were cut in the *XZ* plane. All microstructural observations, photomicrographs and pole figures of EBSD analysis are presented in *XZ*-sections unless otherwise noted.

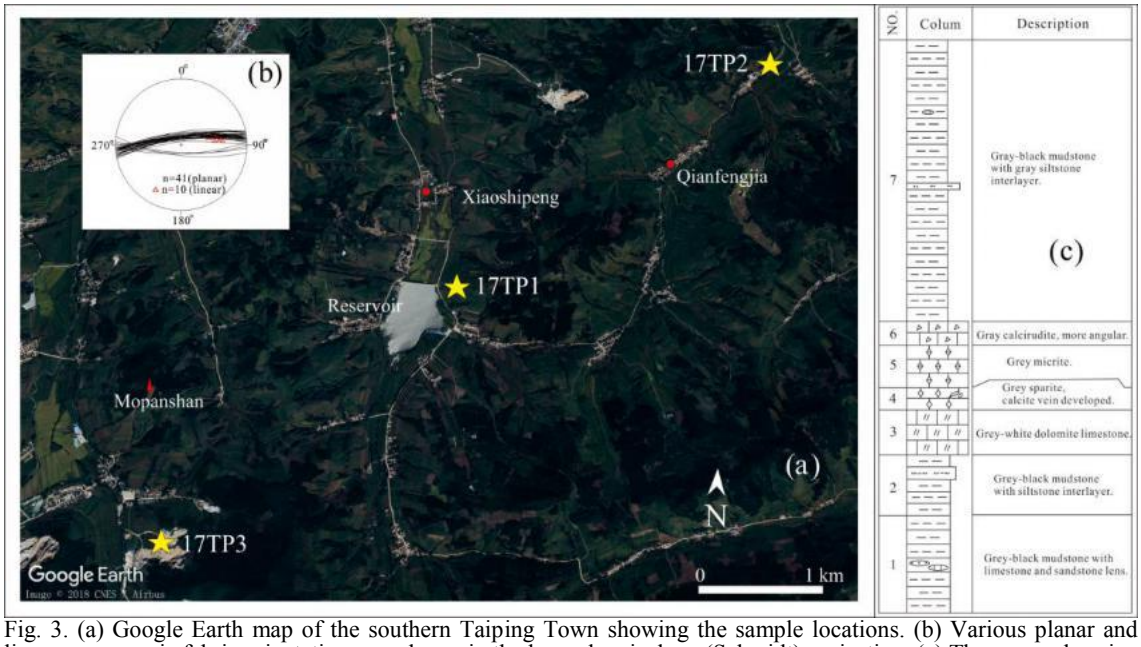

Fig. 3. (a) Google Earth map of the southern Taiping Town showing the sample locations. (b) Various planar and linear mesoscopic fabric orientations are shown in the lower hemisphere (Schmidt) projection. (c) The comprehensive histogram of geochemistry-sedimentary facies of Lower Carboniferous Luquantun Formation (C_1l; modified after Hong et al., 2009).

3 Deformation Mesostructure Characteristics

In the outcrops, we analyzed all the structures of the calcite mylonites shear zone (Xar Moron-Changchun ductile shear zone) at the southern Taiping Town that are subparallel to the margins of the nearly E-W Xar Moron-Changchun Suture Belt (Fig. 2, 4). Outcrop-scale structural features, e.g., shear features, foliations and lineation, were studied and sampling was performed. Calc-silicate minerals are dominated by calcite, quartz and rare muscovite. The numerous calcite mylonites intermittent traced the extension of a dextral shear zone (Fig. 4). Rare mineral-stretching lineations on the bedding and/or foliation planes in the calcite mylonite plunge shallowly to the East or West (Figs. 2b and 4). Table 1 contains a description of the structural and petrological characteristics of the dated samples.

Our field observations around the southern Taiping Town enable us to decipher the main ductile deformation event, namely an E-W dextral shearing. Shear zone fabrics include a significant schistosity and slightly banded structures which exhibit a gneissosity with an E-W trend (355/75 to 88, dip direction/dip) (Figs. 2b and 4). The calcite mylonites (C_1l) developed a planar-linear mylonitic fabrics (Fig. 4). All of these rocks are characterized by high-angle dipped mylonitic foliations and E-W sub-horizontal stretching lineations yielding dextral kinematic indicators. The calcite mylonites are uniformly fine-grained, except coarse-grained porphyroblasts. Strongly stretched and oriented calcites define a foliation oriented parallel to the E-W shear zone. Distinct color banding also defines a macroscopic compositional foliation (Fig. 4j, g; Table 1). They define a weak foliation and faintly visible mineral lineation with some calcite and fine quartz grains (Fig. 4f, h). Dextral shearing can be observed at both the outcrop and thin section scales. At the outcrop-scale, the dextral criteria include centimeter-scale asymmetric σ-type calcite aggregates and elongated quartz rods (up to 2 cm) (Figs. 4a-d, i).

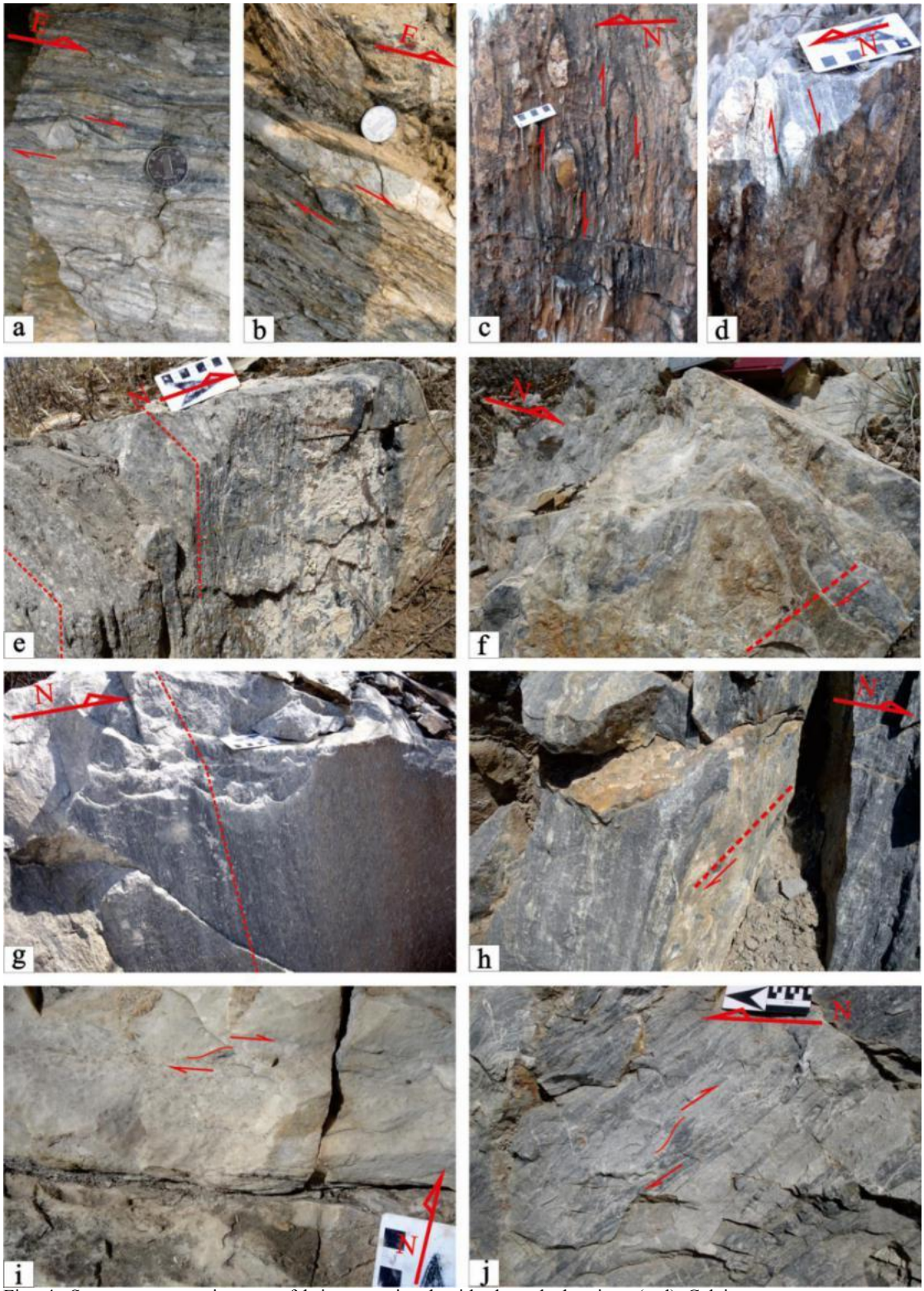

Fig. 4. Some representative mesofabrics associated with dextral shearing. (a-d) Calcite σ-type augen structure indicating a dextral shear along an E-W striking shear zone. (e, g) Gneissosity in calcite mylonites; (f, h) Intermittent lineation developed in calcite mylonites. (i-j) Calcite σ-type augen structure indicating dextral shear sense. a-h are taken form 17TP1, i and j are captured in 17TP2 and 17TP3, respectively.

Table 1. Characteristics of typical calcite mylonites recognized within the Xar Moron-Changchun dextral shear zone.

Sample NO.	Latitude	Longitude	Structures	Description

17TP1–1	N 43°22′24.5″	E 125°45′29.0″	Strongly stretched and oriented calcites define a foliation oriented parallel to the E-W shear zone. Some calcite and fine quartz grains define weak lineation. Large recrystallized quartz σ-clasts was observed. Calcite grains showing a σ-structure.	Distinctly banded layer of brownish color. Grey impure massive calcite mylonite with a few intercalations of thin boundinaged mm-thick quartz-rich aggregates or zones. It was composed mainly of large twinned calcite and subordinate quartz. Quartz grains range from 0.5 to 10 mm, display undulose extinction and frequently have embayments of fine-grained calcite.
17TP1–2			Distinct banding structures. The band containing large (up to 2 cm) recrystallized quartz and calcite σ-clasts were observed. They define a weak foliation and faintly visible mineral lineation.	Impure massive calcite mylonite of pale brown color irregularly intercalated with calc-silicate bands. A few thicker bands can be traced horizontally through the shear zone. The calc-silicate bands consist of mm-sized twinned calcite and elongated quartz clasts.
17TP1–3			Elongated aggregates (up to 1 cm) of quartz are aligned parallel to the shear zone boundary, defines weak foliation. Faintly visible mineral lineation.	Finely banded (spacing < 2 mm) intercalations of calc-silicate and calcite mylonite. Calc-silicate layers consist of 20% rounded quartz grains 0.5–0.8 mm in size, 80% large (up to 5 mm) strongly-twinned calcite grains. Quartz grains display undulose extinction and frequently have embayments of fine-grained calcite.
17TP1–4			A weak foliation defined by aligned fine calcite grains. No visible mineral lineation.	Pure massive calcite mylonite consists of mm-sized twinned and elongated calcite grains.
17TP1–5			A few large (up to 1 cm) recrystallized quartz and calcite σ-clasts were observed. No distinct foliation or lineation was observed.	Finely banded (< 2 mm) calcite mylonite consists of 80% large strongly-twinned calcite grains, 10% large (up to 0.5 mm) quartz grains or aggregates. Muscovite is an accessory mineral.
17TP2–1	N 43°23′50.1″	E 125°47′56.3″	A weak foliation defined by aligned calcite grains. No lineation identified.	Fine-grained, relatively pure calcite mylonite of pale grey color. Approximately equigranular calcite grains up to 1 cm in diameter, straight grain boundaries and heavily twinned.
17TP3–1	N 43°21′06.2″	E 125°43′42.9″	Color banding defines a macroscopic compositional foliation.	Grey impure massive calcite mylonite with a few mm-thick quartz-rich zones. Composed mainly (95–98%) of large twinned calcite and subordinate quartz. Thicker bands can be traced horizontally through the entire shear zone.

4 Deformation Microstructures

In thin sections, classical shear criteria, such as millimeter-scale asymmetric σ-type quartz and calcite grains (Fig. 5a, e, f) confirm the dextral sense of shear. Based on the appearance of the twins, calcite can be classified into four types that correspond to broad ranges of deformation temperatures (Burkhard, 1993; Craddock et al., 2007). Type I: Thin twins, straight, rational; 1, 2 or 3 sets per grain; developed under very weak deformation, at a very low temperature, < 200°C. Type II: Thick twins (>>1 μm), parallel-sided, to slightly lens-shaped, developed under moderate deformation, in the temperature range: 150–300°C. Type III: Curved thick twins, twins in twin, irrational, developed under significant deformation, at temperatures >200°C. Type IV: Thick, patchy, sutured twin boundaries, irrational orientation, developed under strong deformation, at temperatures >250°C, often associated with dynamic recrystallization (Ferrill, 1991, 1998; Ferrill et al., 2004; Vernon, 1981). Thin twins (~0.5±5.0 μm) are dominant in our sample suite, which is a characteristic of calcite deformed around 200–300 °C, see below (Ferrill, 1991, 1998; Ferrill et al., 2004; Vernon, 1981; Table 2). In this study, the microstructures and textures of a natural shear zone in calcite mylonites are analyzed. The reasons that the shear zone have narrowed and deformation has become localized will be explained and interpreted.

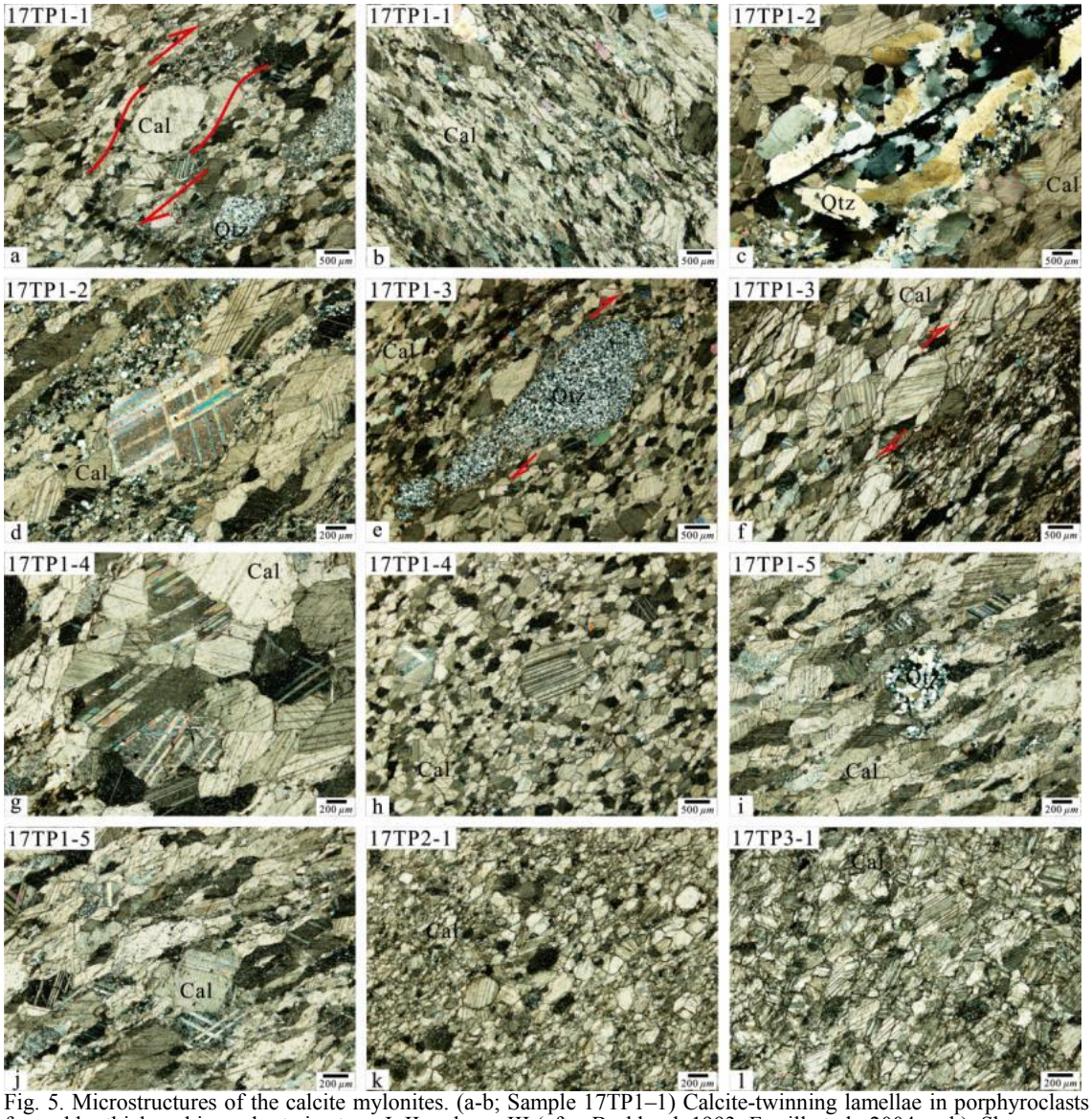

Fig. 5. Microstructures of the calcite mylonites. (a-b; Sample 17TP1–1) Calcite-twinning lamellae in porphyroclasts formed by thick and irregular twins type-I, II and rare III (after Burkhard, 1993; Ferrill et al., 2004; a, b). Shear sense (dextral) is given by `σ-shaped' calcite grains embedded within the calcite matrix (a). (c-d; Sample 17TP1–2) Calcite-twinning lamellae in porphyroclasts formed by thick twins type-II which enclosed twins type-I. The porphyroclasts have elongated shape and they define the oblique foliation. Coarse-grained mylonite (quartz and calcite) shows a variable intensity of dynamic recrystallization; coarse-grained porphyroclasts are elongated and show a shape preferred orientation, with one dominant twin set clockwise oriented to the reference plane. (e-f; Sample 17TP1–3) Quartz-ribbon is interlayered between mylonites showing dextral shear sense. Calcite-twinning lamellae in porphyroclasts formed by twins type-II and I. (g-h; Sample 17TP1–4) Calcite grains showing two sets of twins, note relatively thin and thick straight twins which enclosed twins type-II and I. (i-j; Sample 17TP1–5) Calcite-twinning lamellae in porphyroclasts formed by twins type-II and I. The porphyroclasts have elongated shape and they define the oblique foliation. Dynamic recrystallization of quartz grains are elongated and show a shape preferred orientation. (k; Sample 17TP2–1) Calcite-twinning lamellae in porphyroclasts formed by twins type-II and I. (l; Sample 17TP3–1) Coarse-grained mylonites show small mount of dynamic recrystallization with undulatory extinction; coarse grains are elongated with one dominant twin set approximately parallel to the foliation. In all microphotographs, sample numbers are shown in the upper left corner. All micrographs were taken with crossed polarizers.

Table 2. Deformation features of typical calcite mylonites recognized within the Xar Moron-Changchun dextral shear zone at southern Taiping Town.

Sample NO.	Calcite twin type (Burkhard, M., 1993; Ferrill, 1991)	Type of quartz recrystallization	Geometry description	Temperature/ °C
17TP1–1	Type Ⅰ, Ⅱ	Bulges and recrystallization, undulatory extinction	Thin twins, straight, rotional, 1,2,3 sets per grain; little deformation, little cover, very low temperature.	＜200℃
17TP1–2	Type Ⅰ, Ⅱ	Bulges and recrystallization, undulatory extinction	Thick(＞＞1μm), straight, slightly lense shaped, rational; considerable deformation; 1, 2, 3 sets per grain.	＞200℃

17TP1–3	Type Ⅰ, Ⅱ	Bulges and recrystallization, undulatory extinction	1, 2, 3 sets per grain. thick(＞＞1μm), straight, slightly lense shaped; considerable deformation.	＞200℃
17TP1–4	Type Ⅰ, Ⅱ, small amount of type Ⅲ		Thick(＞＞1μm), straight, slightly lense shaped, rational; considerable deformation; 1, 2, 3 sets per grain; some with curved thick twins; considerable deformation.	＞200℃
17TP1–5	Type Ⅰ, Ⅱ	Bulges and recrystallization, undulatory extinction	Thin twins, straight, rotional, 1,2,3 sets per grain. thick(＞＞1μm), straight, slightly lense shaped.	＞200℃
17TP2–1	Type Ⅰ, small amount of type Ⅱ		Thin twins, straight, rotional, 1 or 2 sets per grain; little deformation, very low temperature; part grains with thick(＞＞1μm), straight, slightly lense shaped twins.	~ 200℃
17TP3–1	Type Ⅱ		Thick(＞＞1μm), straight, slightly lense shaped, rational; considerable deformation, completely twinned grains.	150–300℃

The orientation of the calcite and dolomite layers is easily visible in hand specimens by color contrast of creamy dark impure dolomite with some calcite (Fig. 4) and white pure calcite. The shear zone grades into a discontinuity. As no stretching lineation can be observed, the sample has been cut mutually perpendicular to the foliations in order to undertake a detailed study. All analyzed samples display a single, homogeneous developed and penetrative mylonitic foliations. In the thin section scale, foliation is commonly defined by thin and discontinuous grains and/or the shape preferred orientation of calcite grains and/or by the boundary between pure calcite domains with contrasting grain sizes.

Strongly foliated calcite mylonites have a S-L tectonic fabric characterized by mantle microstructures and rotational porphyroblasts bounded by the same size recrystallized grains of calcite or quartz with lobate grain boundaries (Fig. 5a, e, f, h, i). 90% of the calcite observed in optical microscopy images exhibit prominent twinning (Fig. 5). Twinning is accomplished usually with one or two sets of twins, although grains with a single twin set are more common. Grains with three twin sets rarely occur. Most twins are rational with smooth and straight boundaries and terminate at grain margins revealing that they were formed during the final deformation stages (Burkhard, 1993; Lafrance et al., 1994). These twins correspond to geometric types I and II described by Burkhard (1993). However, type II twins are dominant. Bent and twinned twins (type III; nomenclature after Ferrill et al., 2004) are also observed in a few grains, and these twins with serrated or irregular boundaries are common. These morphological features indicate that twinning occurred mainly at deformation temperatures between 200 °C and 300 °C (Burkhard, 1993; Ferrill et al., 2004).

Samples consist mainly of relatively coarse-grained calcites with a mean grain size of 200–500 μm (Fig. 5). Large grains (calcite porphyroclasts) are moderately elongated (Fig. 5) with a mean aspect ratio (long axis/short axis) ranging from 1.5 to 5.6, highly strained. The long axes of the elongated grains are approximately parallel to the main foliation plane and low angle orientated anticlockwise to the shear zone boundaries (Fig. 5) and define an oblique foliation consistent with a dextral sense of shear (Fig. 5). Large calcite grains show a high density of Type I, II and rare III twins (Fig. 5). Type III twins (Ferrill et al., 2004) are still present in the porphyroclasts but they are less intense and generally only one set of twins orientated anticlockwise to the shear zone boundaries is well preserved (Fig. 5a). The twins terminate at grain boundaries or taper towards the interior of grains (Type III; Fig. 5a). Most of the twin lamellae are slightly curved (Figs. 5a-f). Many porphyroclasts show a characteristic symmetrical undulate extinction by the movement of conjugate extinction bands through the grain interior. All the samples consist of c. 5% recrystallized grains (area occupied by grains<40 μm in diameter; Fig. 5). Recrystallization in a strong deformation area is concentrated along the boundaries of large calcite porphyroclasts and locally along the borders of twin lamellae (Figs. 5a, h). Recrystallized grains (10–50 μm) are equigranular to polygonal in shape, with straight to slightly curved grain boundaries (Fig. 5); they display neither undulatory extinction, twins, nor subgrains (Fig. 5a). Triple grain junctions are frequent (Fig. 5). These microstructural features provide some indications that static recrystallization and grain growth (annealing processes; Molli et al., 2000, 2011; Barnhoorn et al., 2005) may have occurred after shearing.

A population of small (30 to 100 μm), generally not twinned calcite grains with sharp extinction, commonly decorate the boundaries of large twinned grains (Fig. 5b, c, d). These grains are interpreted as dynamically recrystallized calcite grains. These recrystallized grains replace both the host and twinned parts of the old large grains, which implies that grain boundary recrystallization postdates twinning in these samples. On the ground that our samples are dominated by thick twinning (type II) with evidence of recrystallization at the boundaries of twinned calcite grains, the deformation should have occurred under increasing temperatures (to 300 °C), as pointed out by Ferrill et al. (2004). Generally, these deformation-bands or grains of complete recrystallization are characterized by a smaller grain size (Fig. 5a).

In addition, the tectonic fabrics in weak deformation samples are more homogeneously developed and have a lower percentage of recrystallized grains than the fabrics of strong ones, where strongly deformed calcite mylonites usually have intercalated quartz-ribbons (Fig. 5a, c, d, e, i).

Rare quartz grains (50–150 μm average size) are incorporated in the interior of calcite grains or at grain boundaries. Microstructures observed in quartz grains include lenticular aggregates and polycrystalline ribbons indicating dynamic recrystallization by bulging (BLG; Fig. 5a-e, i-j). All these quartz grains have undulatory extinction with almost the same equant shapes (Fig. 5b, d, j); some dynamically recrystallized quartz grains produce a σ-structure indicating the dextral sense of shear (Fig. 5e).

On the other hand, features related to ductile deformation like curved grain boundaries, undulatory extinction, development of core-mantle structures and mylonitization are likely to be related to greenschist-facies deformation. If these structures had formed during early high-level metamorphism, they would have been annealed, producing straight grain boundaries and absence of undulatory extinction. Another factor supporting deformation during greenschist-facies metamorphism is that the orientation of the recrystallized grain long axes within the host rocks display a top-to-the-east sense of shear.

Based on twin morphology (twins types) as well as on the occurrence of grain boundary recrystallization, it seems that calcite deformation has mainly occurred at temperatures between 200 °C and 300 °C under greenschist-facies implying the last stage of E-W dextral shearing. This agrees with the average twin width and twin intensity in our samples, which suggest twinning occurred at temperatures around 200 °C (Burkhard, 1993; Ferrill et al., 2004).

5 EBSD Fabric Analyses

5.1 EBSD analytical methods

Seven samples for electron-backscatter diffraction (EBSD) fabric analysis of quartz/calcite textures from calcite mylonites were chosen (Table 1, 2), and the locations of the samples are shown in Fig. 2. Thin sections with a thickness of 30 μm were prepared along the direction parallel to the lineation and perpendicular to the foliation (*XZ* section), polished using Kejing UNIPOL-802 precision polishing machine with a colloidal silica solution over 2 h to remove surface damage. The EBSD fabric analysis was carried out in the Key Laboratory of Mineral Resources Evaluation in Northeast Asia, Ministry of Natural Resources, Jilin University, Changchun, Jilin, China using EBSD detector mounted on a tungsten filament EVO MA15 scanning electron microscope (SEM). Highly polished thin sections were put in the scanning electron microscope chamber with a 70° tilt angle and with the rock lineation (structural *X* reference direction) parallel to the SEM *X*-axis. The electron backscatter patterns (EBSP) were acquired at a low acceleration voltage of 15 kV, a beam current of ca. 3.0 nA and a beam working distance of ca. 20–24 mm. Conducting resin taps attached to the sample surface surrounding the measurement area was used to reduce charging effects. The EBSP data acquisition was done using mapping modes. Indexing was accepted when at least six detected Kikuchi bands matched with those in the standard reflector file for the analyzed mineral phases. Indexed points with a Mean Angular Deviation (MAD) larger than 1.2 (between detached and simulated patterns) were eliminated to avoid suspicious indexing. The automated EBSD mapping analysis on predefined sampling grid steps smaller than average quartz/calcite grain size (10–30 μm). Although some small step sizes will produce duplicate measurements in some big grains, the results are statistically reliable. Grain-size histograms (Fig. 6) and crystallographic preferred orientation (CPO) pole figures (Fig. 7) were drawn using the Channel 5 software package (Oxford-HKL). For each sample, the [0001] (c axes) crystallographic directions and planes were plotted in the rock fabric (XYZ) reference frame (Fig. 7). And, the pole figures are presented in the lower hemisphere with equal area stereographic projections and contoured with a half-width of 20° using multiple uniform distribution techniques.

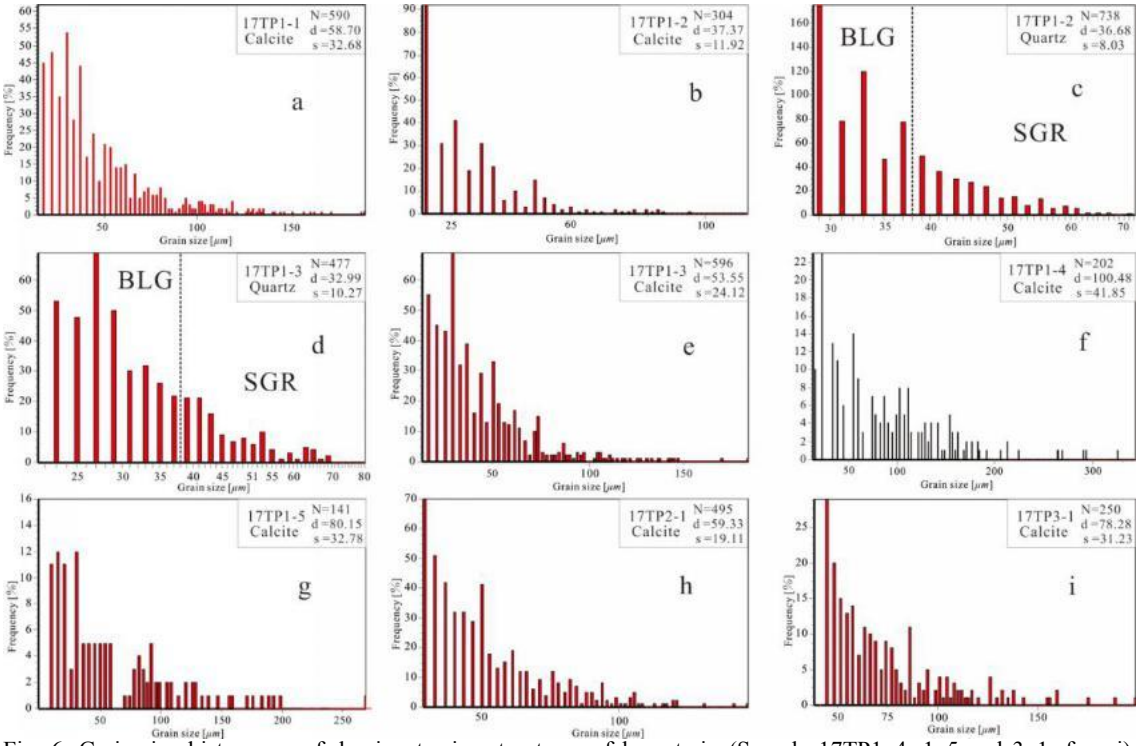

Fig. 6. Grain-size histograms of dominant microstructures of low-strain (Sample 17TP1–4, 1–5 and 3–1; f, g, i), intermediate-strain (17TP1–1, 1–3 and 2–1; a, e, h.) and high-strain (17TP1–2; b) calcite mylonites . N = total number of analyzed grains, d = mean grain size, s = standard deviation. The relation between the particle sizes of recrystallized quartz grain size versus frequency and deformation mechanisms is preserved in c and d (based on Stipp et al., 2010). BLG represents the bulges and recrystallization (280–400 °C), SGR represents the subgrain rotation recrystallization (400–500 °C).

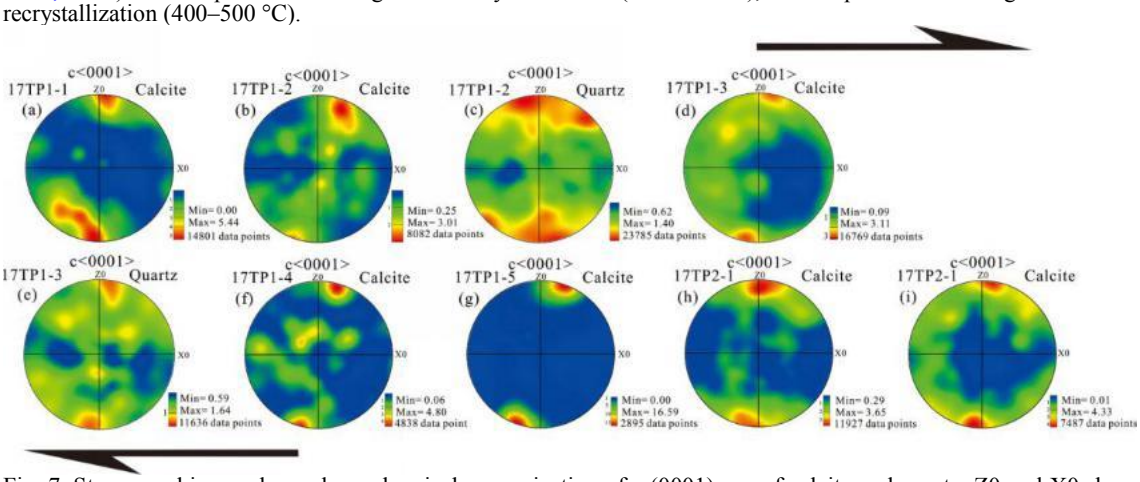

Fig. 7. Stereographic equal-area lower hemisphere projection of c (0001) axe of calcite and quartz. Z0 and X0 show the sample axes. All pole figures indicate an E-W dextral sense of shear.

5.2 EBSD analysis results

The microstructures of the relatively weak deformed calcite mylonites (17TP1–4, 17TP1–5, 17TP3–1) are characterized by coarse calcite grains with a grain size around 80–100 μm (Figs. 6f, g and i). The grain-size-distribution plot shows two peaks, one well defined at 50 μm and the other less pronounced at 100 μm (Figs. 6f, g and i). Undulatory extinction and the minor presence of subgrain boundaries indicate intracrystalline deformation. Conjugate narrow or tabular twins are observed corresponding to Type I, II and Type III twins respectively (Ferrill et al., 2004; Figs. 5g-j, l). In the intermediate-deformed calcite mylonites (17TP1–1, 17TP1–3, 17TP2–1), the calcite grains are elongate and show strong intracrystalline deformation (Figs. 5a, b, e, f, k). Undulatory extinction and curved twins are common. Locally, sutured twin and grain-boundaries can be observed (Figs. 5b, f). Larger calcite grains are surrounded by recrystallized grains with a similar size as the subgrains, creating a core-mantle structure (Fig. 5a). The average grain size is around 58.70 μm, 53.55 μm, and 59.33 μm (Figs. 6a, e, h). In the relatively strong deformed calcite, mylonite (17TP1–2) shows intensely deformed calcite grains that partly contain

wedge-shaped twins (Figs. 6c, d). The larger calcite grains are surrounded by recrystallized grains with similar average grain size (Fig. 5d). The strong deformation calcite mylonite consists of equigranular calcite (Figs. 5c, d). The grain size ranges between 28 μm and 92 μm, with an average of 37.37 μm (Fig. 6b).

In all samples, calcite represents 80–90% of the total rock composition, and some samples include quartz aggregates (17TP1–1, 17TP1–2, 17TP1–3, 17TP1–5). It is interesting to note that the average quartz grain size is around 36.68 μm and 32.09 μm (Figs. 6c, d). The frequency maxima and minima correlate with distinct microstructures indicates the dominance of the recrystallization mechanisms of bulging (Stipp et al., 2010; Newman, 1994).

The crystal-plastic deformation of calcite remains active at lower temperatures (T < 300 °C). Therefore, the combination of structural data from calcite mylonites can help to understand the entire deformation history. Seven orientated calcite-rich samples were selected for combined microstructural and crystallographic preferred orientation analysis (Fig. 7). Locations of all samples have been projected in Figs. 2-3.

Both samples show similar c-axis (0001) pole figures (CPO; Fig. 7). The deformed calcite grains show a strong point maximum of C axis inclined to the Z-axis of the pole figure and records therefore a monoclinic symmetry (Fig. 7a, b, d, f-i) and basal <a> glide. Larger grain size and c-axes distribution indicate that quartz recrystallization was dominated by basal <a> gliding (Xu et al., 2009b; Passchier, 1998; Xia and Liu, 2011; Lafrance et al., 1994; Pieri et al., 2001; Trullenque et al., 2006; Austin et al., 2014; Barber et al., 2007; Erskine et al., 1993). The asymmetry and obliquity of EBSD fabrics indicate a shear direction of the hanging wall towards the E (Fig. 7). All fabrics reflect a deformation environment within low-temperatures and indicate that them formed in greenschist-facies condition.

6 Estimation of Finite Strain and Kinematic Vorticity

Significant ductile shear indicators have been observed in all oriented thin sections, which are parallel to the stretching lineation and perpendicular to the foliation (*XZ* plane) (see above). All these indicators can be used to estimate the strain of the ductile shear zone, presented by two-dimensional kinematic vorticity and finite strain analysis (Passchier and Simpson, 1986; Passchier and Urai, 1988; Xypolias and Doutsos, 2001). All measurements were done on polished hand specimen surfaces parallel to the lineation and normal to the foliation (*XZ*) and normal to lineation and foliation (*YZ*) (Xypolias and Doutsos, 2001).

6.1 Finite strain measurements

Selecting a suitable strain marker is the key to strain measurement. In this study, however, most of the calcite grains are generally fine-medium and have boundaries and shapes which are very easily determined. Therefore, we selected calcite as a strain marker that is larger and easier to measure on a polished hand specimen surface. Although the strain intensity recorded by calcites may be less than that of the whole rocks, it is suitable to compare strain parameters, such as strain types, intensity, and kinematic vorticity, of various rock types in a ductile shear zone, particularly the spatial distribution and variation of the strain parameters.

Two-dimensional strain measurement is generally conducted using Fry's method and the long-short axis method. Fry's method and the long-short axis method of finite strain measurement are widely used due to their superiority (Fry, 1979; Stone et al., 1981; Siddans et al., 1984; Zheng and Wang, 2005). The preconditions of finite strain measurement require the mineral grains to be nearly equidimensional and randomly oriented with a non-Poisson distribution. The results of the finite strain measurement reflect the "full rock strain" (Fry, 1979). When the protolith is a limestone without a pre-existing orientated texture and in which the calcite is nearly randomly distributed, the studied rocks can be used for finite strain measurement (Wang et al., 2004, 2007; Zheng et al., 2005; Liang et al., 2011, 2017).

First, two oriented thin sections of the *XZ* and *YZ* planes were prepared and microphotographs were taken of areas with nearly uniformly distributed mineral grains. For the long-short axis method, the center of each calcite grains was marked on the microphotograph using CorelDraw 17. Calcite grains ≥ 50 were selected, and their long axis and short axis were measured, the aspect ratio was calculated, and the *X/Y* and *Y/Z* values were obtained (Table 3). For the Fry's method, the center of each calcite grains was marked on the microphotograph, the center of the microphotograph was chosen as the point of origin for reference, and then the point of origin was moved to each center of the grains in turn using CorelDraw 17, based on the principles of the Fry's method. Because the deformed grains are large and the zoom of a microscope is limited, about 50 grains for each thin section are generally measured, but the results of the measurements are sufficient to deduce the strain. The results are given in Table 3 and are graphically shown in Figure 8.

Table 3. Finite strain results and calculated parameters.

Sample NO.	Fry's method				Long-short axis method			
	$R_{S\text{-}X/Z}$	$R_{S\text{-}Y/Z}$	$R_{S\text{-}X/Y}$	K	$R_{S\text{-}X/Z}$	$R_{S\text{-}Y/Z}$	$R_{S\text{-}X/Y}$	K
17TP1–1	1.61	1.43	1.13	0.33	1.55	1.38	1.12	0.36
17TP1–2	1.72	1.52	1.14	0.31	1.56	1.43	1.09	0.24
17TP1–3	1.89	1.66	1.14	0.25	2.00	1.67	1.20	0.35
17TP1–4	1.77	1.42	1.25	0.64	1.67	1.39	1.20	0.56
17TP1–5	2.10	1.63	1.28	0.51	1.83	1.48	1.24	0.54
17TP2–1	1.76	1.42	1.24	0.60	1.75	1.42	1.23	0.60
17TP3–1	1.90	1.54	1.23	0.48	1.83	1.48	1.24	0.54

All the calculated data have been plotted in Figure 8 using the Flinn diagram. The logarithmic Flinn diagram is an important differentiation of finite strain types. The finite strain types of deformed rocks are uniform, belonging to compression strain, with a K-value (K=ln (X/Y) / ln (Y/Z)) less than 1 with a range of 0.24–0.64 (Fig. 8a). All the deformed granitic rocks are characterized by S-L-type tectonites.

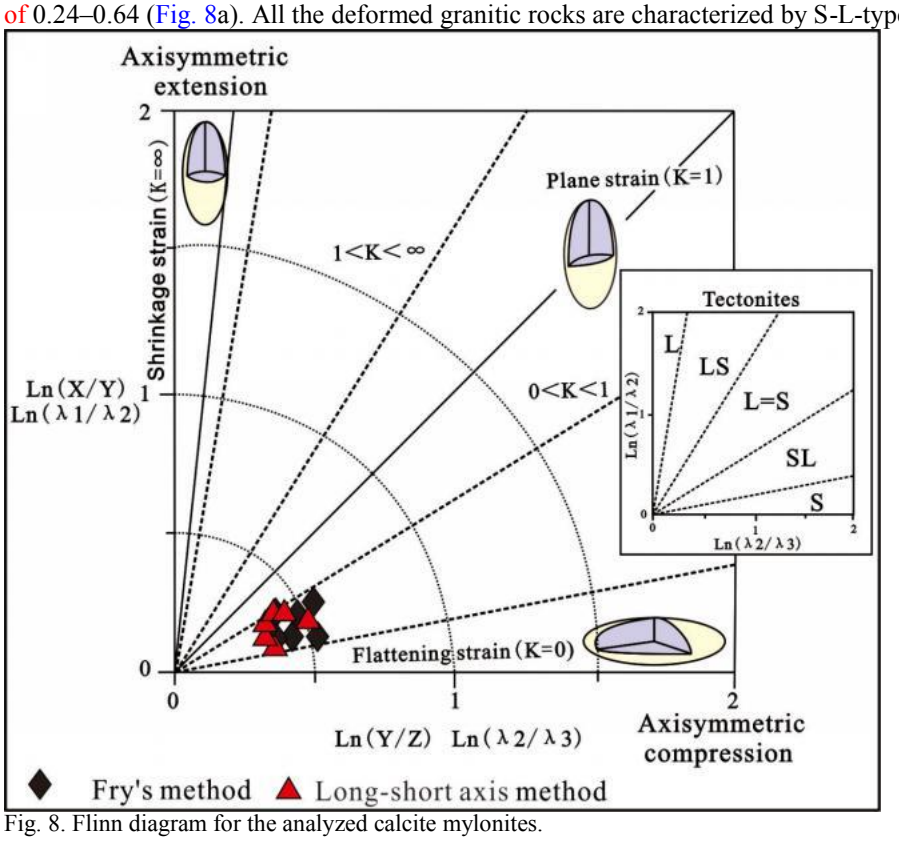

Fig. 8. Flinn diagram for the analyzed calcite mylonites.

6.2 Estimation of shear strain

The twin formation leads to a strain hardening effect, where further strain is accommodated by either increase in twin thickness or twin density depending on the temperature of deformation (Kollmeier et al., 2000; Ferrill, 1998; Groshong, 1972; Craddock and van der Pluijm, 1999; Oesterling et al., 2007).

The number of twin lamellae in a calcite grain is usually expressed in terms of twin intensity (number of twin planes/mm). The intensity is estimated by dividing the number of twins in a set by the width of the host grain, measured perpendicular to the twins (Fig. 9a, b). The "mean twin intensity" for a sample is calculated by averaging the twin-set averages of all twin sets measured in the sample (Fig. 9b). However, at temperatures above 200 °C, calcite shows thick twins and low twin intensities (Fig. 9a). Thus, calcite twin strain can accumulate by increasing the number of twins (twin intensity), increasing the size of twins (i.e., mean twin width, determined by calculating the average of the ratio of the twin width, both the thick and thin and the total number of twins in the set) or both. The relationship between shear strain

accommodated by a calcite twin set, grain size, and twin width is presented by Groshong (1972) and later modified by Ferrill et al. (2004). The relationship is given by:

$\gamma = Tt2\tan(\alpha/2)$

where γ =shear strain; T=twin intensity, t2=mean twin width, and α=angle of rotation of the grain edge from the untwinned to the twinned position and is equal to 38.28° (Fig. 9b; Groshong, 1972; Tripathy and Saha, 2015; Gonzalez-Casado and García-Cuevas, 2002).

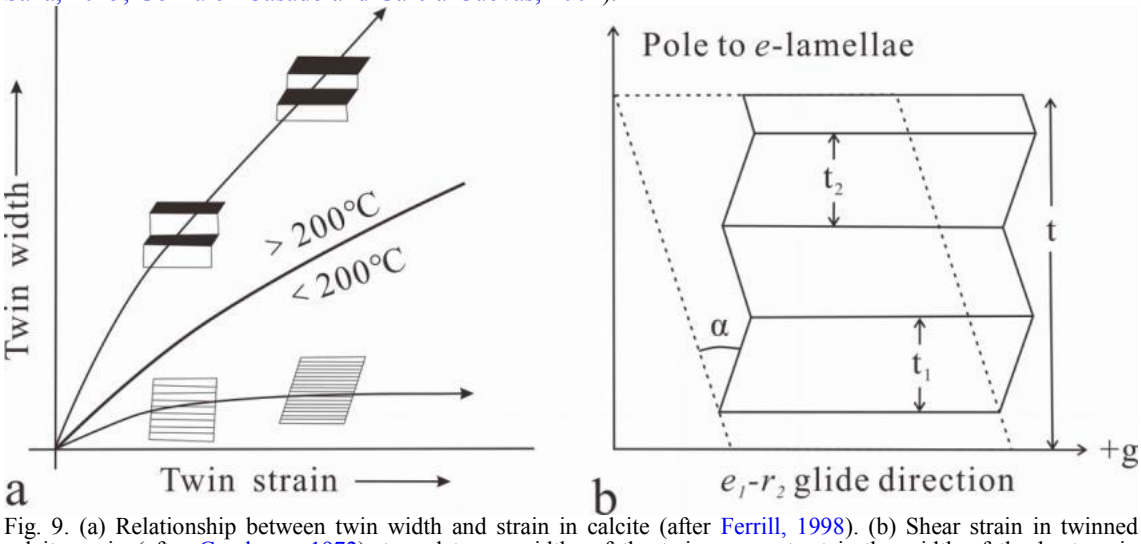

Fig. 9. (a) Relationship between twin width and strain in calcite (after Ferrill, 1998). (b) Shear strain in twinned calcite grain (after Groshong, 1972). t_1 and t_2 are widths of the twin segments; t is the width of the host grain perpendicular to the twin plane; α (=38°17′, Tripathy and Saha, 2015) is the angle of rotation of the grain edge from the untwined to the twinned position.

About 50 grains were measured in each section, with the following parameters determined for each grain: twin lamellae, twin set orientation, twins' average thickness, number of twins and grain width (Table 4).

Table 4. measured hear strain values of calcite mylonites.

Sample NO.	Mean grain size / μm	Twin intensity / T (mm^{-1})	Mean twin width / t (μm)	Shear strain / γ=Tt2tan(α/2)
17TP1–1	58.70	76	6.58	0.17
17TP1–2	37.37	98	4.17	0.14
17TP1–3	53.55	79	5.91	0.16
17TP1–4	100.48	53	12.01	0.22
17TP1–5	80.15	58	10.11	0.20
17TP2–1	59.33	71	7.11	0.18
17TP3–1	78.28	60	9.26	0.19

Most of the calcite grains showed one, two twin sets and a few three sets. The measurements of twins were done without any bias toward twin density, number of sets present or thickness of twins. The mean grain size of calcite samples varied between 37.37 and 100.48 μm (measured by EBSD; Fig. 6). By their appearance, e-twins in the measured calcite samples could be classified as type I to type III twins (Fig. 5), suggesting deformation at temperatures around 200–300°C (Burkhard, 1993; Ferrill et al., 2004). The mean twin width (t), grain size, twin intensity (T) and the calculated shear strain (γ) were obtained from *XZ* plane. The shear strain values are similar with the rang of 0.14–0.22 (Table 4). It is noteworthy that larger grain size is associated with a greater twin width. Similarly, the twin intensity decreases with increasing twin width. The plot of grain size vs twin density (twins/mm) shows that the twin density decreases with increasing grain size, i.e. twinning is grain-size dependent (Rowe and Rutter, 1990; Tripathy and Saha, 2015).

6.3 Kinematic vorticity

The kinematic vorticity value (*Wk*) is a dimensionless measure, defined as the non-linear ratio of pure shear and simple shear components of the deformation (Means, 1994; De Paor, 1983; Reston, 1990; Forte and Bailey, 2007; Passchier, 1987). The shear types of mylonite during its formation can be quantitatively described by kinematic vorticity: $Wk = \cos\alpha$, where α is the angle between the eigenvectors or apophyses

(Simpson and De Paor, 1993; Means et al., 1980). When the components of simple shear are the same as the components of pure shear, the value of *Wk* is 0.75 (Simpson and De Paor, 1993), above which the shear-type is simple-shear dominated general shear, and below which the shear-type is pure-shear dominated general shear.

A number of well-developed techniques and methods have been used to quantitatively assess kinematic vorticity in natural shear zones (Passchier and Simpson, 1986; Passchier and Urai, 1988; Simpson and De Paor, 1993; Zhang and Zheng, 1997). In this study, we calculated kinematic vorticity based on the orientation of recrystallized calcite grains within oblique grain shape fabrics which were used to obtain estimates of flow vorticity during mylonitization in the studied shear zones. All vorticity analyses are also based on the fact that mylonitic foliation is parallel to the shear plane. Results of our analyses are expressed in terms of sectional kinematic vorticity number, *Wn*, (Passchier and Simpson, 1986; Passchier and Urai, 1988) and percentage simple shear values.

Kinematic vorticity estimates can also be obtained based on the assumption that the orientations of the long axes of recrystallized grains are parallel to the direction of the instantaneous stretching axis of flow (Wallis, 1995; Spanos et al., 2015; Fig. 10). Lots of experimental studies have demonstrated that recrystallized grains within an oblique grain shape fabric, and their long axes in a fixed orientation which progressively rotate towards parallelism with the shear plane (Dell'Angelo and Tullis, 1989; Ree, 1991; Herwegh and Handy, 1998; Spanos et al., 2015). Notably, this assumption has been extensively used to estimate kinematic vorticity in quartz tectonites (e.g., Weijermars, 1991, 1993, 1998; Xypolias and Doutsos, 2001; Law et al., 2004; Zheng and Wang, 2005, 2007; Xypolias, 2009; Liang et al., 2015). Thus, it is reasonable to extend this approach to the analysis of calcite tectonites since the mechanism of formation of oblique foliation is similar to both rock types (Passchier, 1998; Spanos et al., 2015). Therefore, we suggest that the greatest recorded angle, δ, between the oblique grain shape fabric and the mylonitic foliation or shear plane can be used to estimates the kinematic vorticity (Fig. 10a). This reveals that the kinematic vorticity, Wn, can be estimated by applying the relationship $Wn = \sin(2\delta)$ (Xypolias, 2010 and references therein). At least 50 orientation measurements of the long axes of grains recrystallized oblique to the mylonitic foliation were taken to determine the angle δ in all *XZ* thin sections (see Xypolias et al., 2013 for a similar case in quartz tectonites). As illustrated in Fig. 5, the obtained δ angles range between 24° and 42° (Table 5). This yields *Wn* estimates of 0.41–0.67 (or 27–46% simple shear). Kinematic vorticity analysis showed that the simple shear component of ductile shearing ranges between 27–46%, which represents or records instantaneous sensitive features of ductile deformation during final deformation.

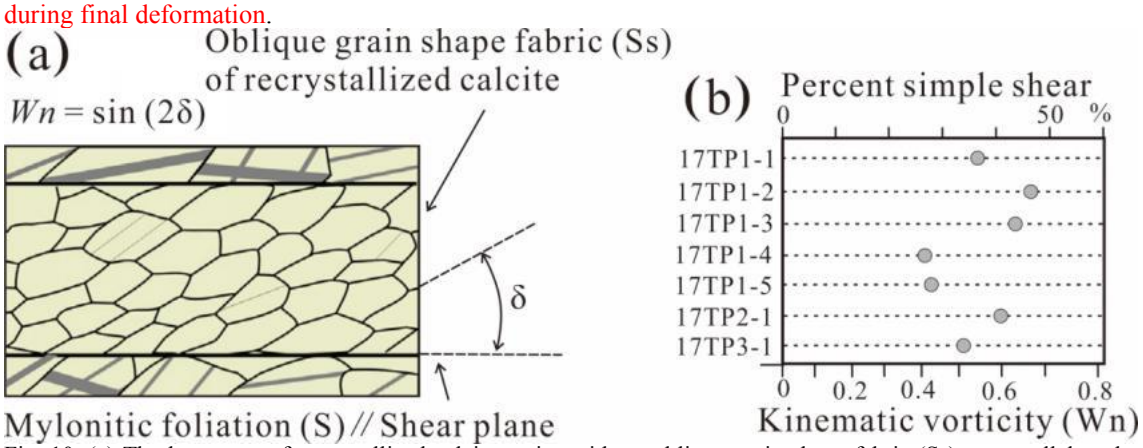

Fig. 10. (a) The long axes of recrystallized calcite grains with an oblique grain shape fabric (Ss) are parallel to the instantaneous stretching axis. The angle, δ, is between the Ss and the mylonitic foliation, S, or shear plane. (b) Vorticity estimates plotted against the relative structural position of samples.

Table 5. Kinematic vorticity data for the analyzed calcite mylonites.

Sample NO.	δ	Vorticity analysis	Percent simple shear
17TP1–1	33.41	0.55	37
17TP1–2	42.19	0.67	46
17TP1–3	39.24	0.63	42
17TP1–4	24.07	0.41	27
17TP1–5	25.76	0.43	28
17TP2–1	36.87	0.60	41
17TP3–1	30.55	0.51	34

7 Rheological Parameters

Some experimental studies of dynamically recrystallized grains were carried out to simulate the development of natural microstructures in deformed rocks and to understand their formation conditions (e.g., Kruhl et al., 1995; Kruhl, 1996; Kruhl and Nega, 1996; Takahashi et al., 1998; Boutonnet et al., 2013; Wang et al., 2011; Zhang et al., 2006; Austin and Evans, 2007; Burkhard, 1993; Parlangeau et al., 2018), such as temperatures, differential stresses and paleo-strain rates.

Differential stresses are calculated with the paleopiezometer of Twsis (1977): $\sigma=750*d^{-0.68}$, where d is from the EBSD analysis (Fig. 6). Paleo-strain rates are one key to understand deformation processes in the ductile shear zone. Insofar as steady-state, intracrystalline plasticity mechanisms are involved, the most suitable form of flow law for extrapolation is generally agreed to be: $\varepsilon = A\sigma^n \exp(-Q/RT)$, (e.g., Poirier, 1985; Hacker et al, 1990; Paterson and Luan, 1990; Hirth et al., 2001; Rutter and Rullis, 2004a, b; Boutonnet et al., 2013; Laurent et al., 2000), where ε is the paleo-strain rate (s^{-1}), σ *is* the differential stress (MPa), A is experiment parameter ($MPa^{-1}s^{-1}$); Q is activation energy ($Jmol^{-1}$); T is temperature (K); ideal gas constant R= $8.314JK^{-1}mol^{-1}$; n is stress exponent. Based on paleopiezometer of Heard and Raleich (1972), $A=6\times10^{-18}$; Q=62000; n=8.3.

Mineral deformation behaviors, c-axis EBSD fabrics and quartz grain size-frequency diagrams demonstrate that the ductile shear zone developed under greenschist-facies conditions, with deformation temperatures ranging from 200 to 300 °C, and dislocation creep as the main deformation mechanism (more details see above and discussion). We constructed paleo-strain rates with differential stress according to Twsis (1977) at temperatures of 200 °C and 300 °C (Table 6).

The average size is in the range of 37.37 to 100.48 μm, with differential stress ranging between 32.63 and 63.94 MPa using the equations of Twiss (1977). For strain rate estimates, there are no great differences between the two groups of differential stresses (Table 6). At 200 °C deformation conditions, the paleo-strain rate estimates using flow law are in the range of 8.62×10^{-10} to 3.24×10^{-12} S^{-1}. At 300 °C deformation conditions, paleo-strain rates are in the range of 1.33×10^{-8} to 5.02×10^{-11} S^{-1}, for further interpretations see below.

Table 6. Estimates of differential stresses (MPa) and paleo-stain rates (s^{-1}).

Sample NO.	T / °C	Mean grain size d / μm	σ/MPa Twsis, 1977 $\sigma=750D^{-0.68}$	ε=Aσ^{n}exp[–Q/RT] Heard and Raicigh, 1972
17TP1–1	200	58.7	47.03	6.73755E–11
	300			1.04272E–09
17TP1–2	200	37.37	63.94	8.61738E–10
	300			1.33365E–08
17TP1–3	200	53.55	50.06	1.1313E–10
	300			1.75082E–09
17TP1–4	200	100.48	32.63	3.24308E–12
	300			5.01907E–11
17TP1–5	200	80.15	38.05	1.16162E–11
	300			1.79775E–10
17TP2–1	200	59.33	46.69	6.34359E–11
	300			9.81749E–10
17TP3–1	200	78.28	38.67	1.32718E–11
	300			2.05398E–10

8 Discussion and Interpretation

Our structural, textural investigations presented above to allow us to discuss the characteristics and deformation mechanism of calcite mylonites in the Xar Moron-Changchun dextral shear zone and its implication for the Triassic tectonic evolution of Northeastern China.

8.1 Deformation characteristics and temperature

All the rocks seem to have undergone deformation under conditions of relative weak deformation. Irregular twin boundaries due to twin boundary migration reflect deformation at a temperature well around 200 to 300°C (Burkhard, 1993). The asymmetric (σ-structure) calcite/quartz grains or aggregates with wedge-shaped appendages correspond to a top-to-E shear direction shearing during crystal plastic deformation (Fig. 5a). The 2-dimensional analysis of the calcite grain shape fabric, finite strain measurements and the calcite CPO reveal a monoclinic fabric symmetry which provides evidence for dominant non-coaxial deformation in the twinning regime (Schmid et al., 1980; Wenk et al., 1987; Borradaileand McArthur, 1990). The complete CPOs have a single strong c-axis maximum around Z-axis. The obliquities of these c-axis girdles (with different orientation with respect to the *XZ*-plane, Fig. 7) also can be related to a specific right-lateral sense of shear. This process is promoted by pervasive dynamic recrystallization (Schmid and Casey, 1986; Michel et al., 2006) with the dominant basal slip system (Fig. 7; Schmid et al., 1987; De Bresser, 1991, 1996; Rogowitz et al., 2016) in a non-coaxial deformation regime with a bulk pure shear-dominated general shear.

It seems probable that the entire calcite mylonite has undergone a component of uplift which led to subhorizontal lifting in an already compressional deformation regime. The strain concentration resulted in the localization of deformation in narrow zones. The S-L-calcite tectonites within the shear zone are probably recording non-coaxial general shearing during this compressional tectonics under greenschist-facies conditions, with the range of deformation temperatures from 200 to 300°C. If we take the average geothermal gradient of 33 °C/ km (average geothermal gradient of the world's continents), it can be roughly inferred that the fine-grained calcite mylonites deformed at shallow crustal depths on the order of 6–9 km.

8.2 Calcite deformation mechanisms

The observed undulose extinction indicates the presence of geometrically necessary dislocations which may cause the development of a CPO (Hirth and Tullis, 1992) which is consistent with dominant basal <a> slip (Barber et al., 2007; De Bresser and Spiers, 1993, 1997). Although dissolution precipitation creep and stress-directed grain growth may also lead to the formation of a weak CPO (Bons and den Brok, 2000; Ebert et al., 2007), these processes are not considered to be responsible for the observed CPO because crystal-plastic deformation can be directly linked with undulose extinction and presence of subgrains. Temperatures above 200°C, which have most likely prevailed in the investigated rocks, already activate dynamic recrystallization in calcite (Herwegh and Pfiffner, 2005; Kennedy and White, 2001; Delle Piane et al., 2008, 2009). These strong deformation zones are characterized by (1) core mantle structure where host grains are surrounded by some small recrystallized grains, (2) an extremely small grain size, (3) grain boundary triple junctions with nearly 120 angles (Figs. 5k, l). Dynamic recrystallization (BLG, bulging recrystallization; SGR, subgrain rotation recrystallization) and the accompanying intracrystalline deformation mechanisms led to grain size reduction and strain localization (White, 1979; Barnhoorn et al., 2004; Blenkinsop, 1991; Craddock and van der Pluijm, 1999; De Bresser et al., 2001; Rocher et al., 2004; Schmalholz and Duretz, 2017). Strong undulose extinction suggests intense intracrystalline deformation within the coarse grains. These subgrains of host grains and surrounding recrystallized grains, slightly curved grain boundaries are probably results of intracrystalline deformation and dynamic recrystallization implying that the deformation took place within the dislocation-creep regime (Bestmann et al., 2000; Wheeler et al., 2001; Casey et al., 1998; Ellis and Stöckhert, 2004; Holyoke et al., 2013).

These predictions about deformation strain rates and differential stresses are in agreement with a deformation temperature approximately 200–300°C. The calculated paleo-strain rates are between $10^{-7.87}$ s^{-1} and $10^{-11.49}$ s^{-1} with differential stresses of 32.63–63.94 MPa (Table 6). At least, the differential stress and strain rate conditions can be enough to represent the lower limit of the deformation conditions. The calculated strain rate lies at the higher bound of typical strain rates in shear zones at crustal levels (Pfiffner and Ramsay, 1982; Lacombe, 2007; Okudaira and Shigematsu, 2012; Ulrich et al., 2002) may indicate a relatively rapid deformation. This ductile shearing at the location of maximal deformation may have been caused by twinning, intracrystalline slip, basal <a> slip systems accompanied by the dynamic recrystallization of SGR and BLG within the dislocation-creep regime.

8.3 Deformation ages along the Xar Moron-Changchun dextral shear zone

The timing of the final closure of the Paleo-Asian Ocean along the Solonker-Xar Moron-Changchun-Yanji suture has been a controversial issue and the various proposals including Middle Devonian to Late Carboniferous or earlier (Tang, 1990; Zhao et al., 2013; Xu et al., 2013, 2015; Chen et al., 2016, 2017), late Early Permian (Feng et al., 2010), or Middle Mesozoic (Nozaka and Liu, 2002). However, abundant new geological, paleobiogeography, lithofacies paleogeography, geochronological, geochemical and paleomagnetic data that have been obtained over the past decades have provided convincing evidence that the final closure of the Paleo-Asian Ocean occurred during the Late Permian-Early or Middle Triassic in a scissor-like style eastwards (Sengör et al., 1993; Xiao et al., 2003, 2015; Sun et al., 2004; Li, 2006; Wu et al., 2007, 2011; Cao et al., 2012, 2013; Eizenhöfer et al., 2014;

Han et al., 2016, 2017; Wang et al., 2015; Du et al., 2017; Li et al., 2014, 2015, 2017; Wang et al., 2017; Zhou et al., 2018; Liu et al., 2017; Guan et al., 2019; JBGMR, 1988, 1997; Jian et al., 2008). Assuming that the Changchun-Yanji suture is the eastern extension of the Solonker-Xar Moron-Changchun suture, preserved relics of the suture should exist in the Changchun area.

Along the Xar Moron-Changchun-Yanji suture, the ductile strike-slip shearing can be observed in all pre-Jurassic units within the fault zone. Triassic granites along the Xar Moron Changchun-Yanji Fault yielded zircon U-Pb ages of 237–229 Ma and displayed the same shearing deformation with obvious E-W striking foliation and sub-horizontal lineation (Li et al., 2007; Li et al., 2014), implying that emplacement of this syn-kinematic pluton was related to the strike-slip shearing (Zhao et al., 2015). Lots of A-type granites which implying a post-collision intraplate tectonic setting also have been found in Late Triassic as an EW trending (e.g., Han et al., 2015, 2017; Song et al., 2018; Zhang and Zhai, 2010). Moreover, several muscovite $^{40}Ar/^{39}Ar$ ages from mylonite and granitic gneiss along the Xar Moron-Changchun Fault have been published with consistent ages of 209–221 Ma (Ma, 2009; Zhao et al., 2015; Zhang et al., 2009a, b, 2010). Lastly, undeformed Early Cretaceous granites intrude the older rocks along the fault zone, especially the O-S rocks and the Late Permian series (Fig. 2, 3; Wu et al., 2005). These thermochronologic results successfully constrain the strike-slip movement most likely in the Late Triassic.

8.4 Constraints of dextral strike-slip shearing

After the end of the CAOB formation that resulted in the amalgamation and compression of the NCC, Tarim Craton, SIB and several intervening microcontinents, intra-continental strike-slip faults are the prominent tectonic features of Central-Eastern Asia during the Early Mesozoic (Lamb et al., 1999; Johnson, 2004; Webb and Johnson, 2006; Webb et al., 2010; Zhao et al., 2013, 2015; Zhai et al., 2004; Zhang et al., 2013; Heumann et al., 2014). The strike-slip faults can be ascribed to the consequence of several tectonic events, such as the southward subduction of the Mongol-Okhotsk Ocean (Meng, 2003; Zorin, 1999; Enkin et al., 1992; Cogné et al., 2005; Liang et al., 2019), the northwestern subduction of Paleo-Pacific plate (Wang et al., 2013; Li et al., 2019), and the far-field effects of the north-directed continental subduction between the NCC-South China Block (SCB) (Rowley et al., 1997; Liu et al., 2006; Meng and Zhang, 1999; Zhang et al., 2013).

Considering these compressional events at the northern NCC and southern margins of Xing'an-Mongolian Orogenic Belt (XMOB), we deduce that this region was under an NNW-SSE compressional and shortening regime (Zhao et al., 2015). The E-W trending dextral strike-slip Xar Moron-Changchun shear zone, which was coeval with magmatic intrusions (Zhang et al., 2012; Wang et al., 2013), formed just in this shortening regime. The main activity age has been constrained to the Late Triassic (Zhang et al., 2002; Ma, 2009; Wang et al., 2013; Zhao et al., 2015). This E-W large-scale strike-slip movement is a consequence of the eastward extrusion of the of XMOB (Zhao et al., 2015), and results from far-field forces associated with Late Triassic convergence domain (Zhao et al., 2015). This large-scale compression might result in the rapid uplift and exhumation of the calcite mylonites, and later stage brittle fractures in this area.

9. Conclusions

In summary, the following conclusions can be drawn from the results of the analysis of structures, microfabrics, EBSD fabrics and paleopiezometry of the Xar Moron-Changchun dextral shear zone:

(1) Mineral deformation behavior, twin morphology, C-axis EBSD fabrics and quartz grain size-frequency diagrams demonstrate that the Moron-Changchun ductile shear zone was developed under conditions of the greenschist facies, with the range of deformation temperatures from 200 to 300 °C. These subgrains of host grains and surrounding recrystallized grains, strong undulose extinction, slightly curved grain boundaries are probably results of intracrystalline deformation and dynamic recrystallization implying that the deformation took place within the dislocation-creep regime at shallow crustal levels.

(2) The asymmetric (σ-structure) calcite/quartz grains or aggregates, asymmetry of calcite c-axes fabric diagrams and the oblique foliation of recrystallized calcite grains correspond to a top-to-E shearing during crystal plastic deformation. The calculated paleo-strain rates are between $10^{-7.87}$ s^{-1} and $10^{-11.49}$ s^{-1} with differential stresses of 32.63–63.94 MPa lying at the higher bound of typical strain rates in shear zones at crustal levels, and may be indicating a relatively rapid deformation. The S-L-calcite tectonites have undergone a component of uplift which led to subhorizontal lifting in an already non-coaxial compressional deformation regime with a bulk pure shear-dominated general shear.

(3) This E-W large-scale dextral strike-slip movement is a consequence of the eastward extrusion of the XMOB which results from far-field forces associated with Late Triassic convergence domain after the final closure of the Paleo-Asian Ocean.

Acknowledgments

This project was financially co-supported by the National Key R&D Program of China (Grant No.

2017YFC0601401) and National Natural Science Foundation of China (Grant no. 41602211 and 41230206). We acknowledge polishing of the English by Qi Zheng from School of Foreign Language Education, Jilin University.

References

Austin, N., and Evans, B., 2009. The kinetics of microstructural evolution during deformation of calcite. *Journal of Geophysical Research*, 114: B9402.

Austin, N., Evans, B., Rybacki, E., and Dresen, G., 2014. Strength evolution and the development of crystallographic preferred orientation during deformation of two-phase marbles. *Tectonophysics*, 631: 14–28.

Austin, N.J., and Evans, B., 2007. Paleowattmeters: a scaling relation for dynamically recrystallized grain size. *Geology*, 35: 343–346.

Bahattacharya, A.R., and Weber, K., 2004. Fabric development during shear deformation in the main central thrust zone, NW Himalaya, India. *Tectonophysics*, 387: 23–46.

Barber, D.J., Wenk, H.R., Gomez-Barreiro, J., Rybacki, E., and Dresen, G., 2007. Basal slip and texture development in calcite: new results from torsion experiments. *Physics and Chemistry of Minerals*, 34: 73–84.

Barnhoorn, A., Bystricky, M., Burlini, L., and Kunze, K., 2004. The role of recrystallisation on the deformation behaviour of calcite rocks: large strain torsion experiments on Carrara marble. *Journal of Structural Geology*, 26: 885–903.

Barnhoorn, A., Bystricky, M., Burlini, L., and Kunze, K., 2005. Post-deformational annealing of calcite rocks. *Tectonophysics*, 403: 167–191.

Bell, T.H., and Johnson, S.E., 1989. The role of deformation partitioning in the deformation and recrystallization of plagioclase and K-feldspar in the Woodroffe Thrust mylonite zone, central Australia. *Journal of Metamorphic Geology*, 7: 151–168.

Bestmann, M., and Prior, D.J., 2003. Intragranular dynamic recrystallization in naturally deformed calcite marble: diffusion accommodated grain boundary sliding as a result of subgrain rotation recrystallization. *Journal of Structural Geology*, 25: 1597–1613.

Bestmann, M., Kunze, K., and Matthews, A., 2000. Evolution of a calcite marble shear zone complex on Thassos Island, Greece: microstructural and textural fabrics and their kinematic significance. *Journal of Structural Geology*, 22: 1789–1807.

Bestmann, M., Prior, D.J., and Grasemann, B., 2006. Characterisation of deformation and flow mechanics around porphyroclasts in a calcite marble ultramylonite by means of EBSD analysis. *Tectonophysics* , 413: 185–200.

Blenkinsop, T.G., 1991. Cataclasis and processes of particle size reduction. *Pure And Applied Geophysics*, 136: 59–86.

Bons, P.D., and den Brok, B., 2000. Crystallographic preferred orientation development by dissolution-precipitation creep. *Journal of Structural Geology*, 22: 1713–1722.

Borradaile, G. J., and McArthur, J., 1990. Experimental calcite fabrics in a synthetic weaker aggregate by coaxial and non-coaxial deformation. *Journal of Structural Geology*, 12(3): 351–363.

Boutonnet, E., Leloup, P.H., Sassier, C., Gardien, V., and Ricard, Y., 2013. Ductile strain rate measurements document long-term strain localization in the continental crust. *Geology*, 41(8): 819–822.

Brodie, K. H., 1980. Variations in mineral chemistry across a shear zone. *Journal of Structural Geology*, 2: 265–272.

Burkhard, M., 1993. Calcite twins, their geometry, appearance and significance as stress-strain markers and indicators of tectonic regime: a review. *Journal of Structural Geology*, 15: 351–368.

Busch, J.P., and Van der Pluijm, B.A., 1995. Calcite textures, microstructures and rheological properties of marble mylonites in the Bancroft shear zone, Ontario, Canada. *Journal of Structural Geology*, 17: 677–688.

Cai, K.D., Sun,M., Buslov,M.M., Jahn, B.M., Xiao,W.J., Long, X.P., Chen, H.Y.,Wan, B., Chen, M., Rubanova, E.S., Kulikova, A.V., and Voytishek, E.E., 2016. Crustal nature and orogin of the Russian Altai: Implications for the continental evolution and growth of the Central Asian Orogenic Belt (CAOB). *Tectonophysics*, 674: 182–194.

Cao, H.H., Xu, W.L., Pei, F.P., Guo, P.Y., and Wang, F., 2012. Permian tectonic evolution of the eastern section of the northernmargin of the North China Plate: Constraints from zircon U-Pb geochronology and geochemistry of the volcanic rocks. *Acta Petrologica Sinica*, 28(9): 2733–2750 (in Chinese with English abstract).

Cao, H.H., Xu,W.L., Pei, F.P.,Wang, Z.W., Wang, F., and Wang, Z.J., 2013. Zircon U-Pb geochronology and petrogenesis of the Late Paleozoic-Early Mesozoic intrusive rocks in the eastern segment of the northern margin of the North China Block. *Lithos*, 170–171: 191–207.

Cao, S., Liu, J., Leiss, B., Neubauer, F., Genser, J., and Zhao, C., 2011. Oligo-Miocene shearing along the Ailao Shan-Red River shear zone: Constraints from structural analysis and zircon U-Pb geochronology of magmatic rocks in the Diancang Shan massif, SE Tibet, China. *Gondwana Research*, 19(4): 975–993.

Cao, S., Neubauer, F., Liu, J., Bernroider, M., Cheng, X., Li, J., and Genser, J., 2017. Rheological weakening of high-grade mylonites during low-temperature retrogression: The exhumed continental Ailao Shan-Red River fault zone, SE Asia. *Journal of Asian Earth Sciences*, 139: 40–60.

Casey, M., Kunze, K., and Olgaard, D.L., 1998. Texture of Solnhofen limestone deformed to high strains in torsion.*Journal of Structural Geology*, 20: 255–267.

Chen, J., Chen, Y., and Wang, Q., 2008. Synthetic informational mineral resource prediction: case study in Chifeng Region, Inner Mongolia, China. *Frontiers of Earth Science*, 15: 18–26 (in Chinese with English abstract).

Chen, N.H.C., Zhao, G.C., Jahn, B.M., Zhou, H., and Sun, M., 2017. Geochemistry and geochronology of the Delinggou intrusion: implications for the subduction of the Paleo-Asian Ocean beneath the north China Craton. Gondwana Research, 43: 178–192.

Chen, Y., Zhang, Z.C., Li, K., Yu, H.F., and Wu, T.R., 2016. Detrital zircon U-Pb ages and Hf isotopes of Permo-Carboniferous sandstones in central Inner Mongolia, China: Implications for provenance and tectonic evolution of the southeastern Central Asian Orogenic Belt. *Tectonophysics*, 671: 183–201.

Cogné, J.P., Kravchinsky, V.A., Halim, N., and Hankard, F., 2005. Late Jurassic-Early Cretaceous closure of the Mongol-Okhotsk Ocean demonstrated by new Mesozoic palaeomagnetic results from the Trans-Baikal area (SE Siberia).*Geophysical Journal International*,163: 813–832.

Craddock, J.P., and van der Pluijm, B.A., 1999. Sevier-Laramide deformation of the continental interior from calcite twinning analysis, west-central North America. *Tectonophysics*, 305: 275–286.

Craddock, J.P., Mckiernan, A.W., and Wit, M.D., 2007. Calcite twin analysis in syntectonic calcite, Cape Fold Belt, South Africa: Implications for fold and cleavage formation within a shallow thrust front. *Journal of Structural Geology*, 29(7): 1100–1113.

Dai, L.M., Li, S.Z., Li, Z. H., Somerville, I.D., Suo, Y.H., Liu, X.C., Gerya,T., and Santosh, M., 2018. Dynamics of exhumation and deformation of hp-uhp orogens in double subduction-collision systems: numerical modeling and implications for the western dabie orogen. *Earth-Science Reviews*, 182: 68–84.

De Bresser, J.H.P., 1991. Intracrystalline deformation of calcite. *Geologica Ultraiectina*, 79: 1–191.

De Bresser, J.H.P., 1996. Steady state dislocation densities in experimentally deformed calcite materials: single crystals versus polycrystals. *Journal Of Geophysical Research*, 101: 22–189.

De Bresser, J.H.P., 2002. On the mechanism of dislocation creep of calcite at high temperature: Inferences from experimentally measured pressure sensitivity and strain rate sensitivity of flow stress. *Journal of Geophysical Research*, 107: 1–16.

De Bresser, J.H.P., and Spiers, C.J., 1997. Strength characteristics of the r, f, and c slip systems in calcite. *Tectonophysics*, 272(1):1–23.

De Bresser, J.H.P., Spiers, C.J., 1993. Slip systems in calcite single crystals deformed at 300–800°C. *Journal Of Geophysical Research*, 98: 6397–6409.

De Bresser, J.H.P., Ter Heege, J.H., and Spiers, C.J., 2001. Grain size reduction by dynamic recrystallization: can it result in major theological weakening? *International Journal of Earth Sciences*, 90: 28–45.

De Paor, D.G., 1983. Orthographic analysis of geologic structures, Deformation theory. *Journal of Structural Geology*, 5: 255–278.

Dell'Angelo, L.N., and Tullis, J., 1989. Fabric development in experimentally sheared quartzites. *Tectonophysics*, 169: 1–21.

Delle Piane, C., Burlini, L., and Kunze, K., 2009. The influence of dolomite on the plastic flow of calcite. *Tectonophysics*, 467: 145–166.

Delle Piane, C., Burlini, L., Kunze, K., Brack, P., and Burg, J.P., 2008. Rheology of dolomite: large strain torsion experiments and natural examples. *Journal of Structural Geology*, 30: 767–776.

Du, Q.X., Han, Z.Z., Shen, X.L., Gao, L.H., Han, M., Song, Z.G., Li, J.J., Zhong,W.J., Yan, J.L., and Liu, H., 2017. Geochemistry and geochronology of Upper Permian-Upper Triassic volcanic rocks in eastern Jilin Province, NE China: implications for the tectonic evolution of the Palaeo-Asian Ocean. *International Geology Review*, 59 (3): 368–390.

Ebert, A., Herwegh, M., and Pfiffner, A., 2007. Cooling induced strain localization in carbonate mylonites within a large-scale shear zone (Glarus thrust, Switzerland). *Journal of Structural Geology*, 29: 1164–1184.

Eizenhöfer, P.R., Zhao, G.C., Zhang, J., and Sun, M., 2014. Final closure of the Paleo-Asian Ocean along the Solonker Suture Zone: Constraints from geochronological and geochemical data of Permian volcanic and sedimentary rocks. *Tectonics*, 33: 441–463.

Ellis, S., and Stöckhert, B., 2004. Elevated stresses and creep rates beneath the brittle-ductile transition caused by seismic faulting in the upper crust. *Journal of Geophysical Research: Solid Earth*, 109: 1–10.

Enkin, R.J., Yang, Z.Y., Chen, Y., and Courtillot, V., 1992. Paleomagnetic constraints on the geodynamic history of the major blocks of China from the Permian to the present. *Journal of Geophysical Research: Solid Earth,* 97(B10): 13953–13989.

Erskine, B.G., Heidelbach, F., and Wenk, H.R., 1993. Lattice preferred orientations and microstructures of deformed Cordilleran marbles: correlation of pure shear indicators and determination of strain path. *Journal of Structural Geology*, 15: 1189–1205.

Feng, G.Y., Liu, S., Zhong, H., Jia, D.C., Qi, Y.Q.,Wang, T., and Yang, Y.H., 2010. Geochemical characteristics and petrogenesis of late Paleozoicmafic rocks fromYumuchuan, Jilin Province. *Geochimica*, 39: 427–438 (in Chinese with English abstract).

Ferrill, D. A., 1991. Calcite twin widths and intensities as metamorphic indicators in natural low-temperature deformation of limestone. *Journal of Structural Geology*, 13(6): 667–675.

Ferrill, D. A., Morris, A. P., Evans, M. A., Burkhard, M., Groshong, R.H., and Onasch, C.M., 2004. Calcite twin morphology: A low- temperature deformation geothermometer. *Journal of Structural Geology*, 26: 1521–1529.

Ferrill, D.A., 1998. Critical re-evaluation of differential stress estimates for calcite twins in coarse-grained limestone. *Tectonophysics*, 285: 77–86.

Forte, A.M., and Bailey, C.M., 2007. Testing the utility of the Porphyroclast hyperbolic distribution method of kinematic vorticity analysis. *Journal of Structural Geology*, 29: 983–1001.

Fry, N., 1979. Random point distributions and strain measurements in rocks. *Tectonophysics*, 6: 89–105.

Gonzalez-Casado, J.M., and García-Cuevas, C., 2002. Strain analysis from calcite e-twins in the Cameros basin, NW Iberian Chain, Spain. *Journal of Structural Geology*, 24: 1777–1788.

Groshong, R.H., Jr., 1972. Strain calculated from twinning in calcite. *Geological Society of America Bulletin*, 83: 2025–2038.

Guan, Q.B., Liu, Z.H., Liu, Y.J., Liu, J., Wang, S.J., and Tian, Y., 2019. Geochemistry and zircon U-Pb geochronology of mafic rocks in the Kaiyuan tectonic mélange of northern Liaoning Province, NE China: Constraints on the tectonic evolution of the Paleo-Asian Ocean, *Geological Journal*, 54: 656–678.

Guo, B., Liu, S., Zhang, J., and Yan, M., 2015. Zircon U-Pb-Hf isotope systematics and geochemistry of Helong granite-greenstone belt in Southern Jilin Province, China: Implications for Neoarchean crustal evolution of the northeastern margin of North China Craton. *Precambrian Research*, 271: 254–277.

Hacker, B., Yin, A., Christie, J.M., and Snoke, A.W., 1990. Differential stress, strain rate, and temperatures of mylonitization in the Ruby Mountains, Nevada: Implications for the rate and duration of uplift. *Journal of Geophysical Research*, 95(B6): 8569–8580.

Han, J., Zhou, J.B.,Wang, B., and Cao, J.L., 2015. The final collision of the CAOB: constraint from the zircon U-Pb dating of the Linxi Formation, Inner Mongolia. *Geoscience Frontiers*, 6: 211–225.

Han, Z.Z., Song, Z.G., Gao, L.H., Han, M., Guo, Z.P., Zhong, W.J., Li, J.J., Du, Q.X., Yan, J.L., and Liu, H., 2017. Late Paleozoic volcanic events in "Daheishan Horst" in Jilin, China and their tectonic significance. *Earth Science Frontiers*, 24 (2): 186–201 (in Chinese with English abstract).

Han, Z.Z., Zhong,W.J., Gao, L.H., Han, M., Yan, J.L., and Liu, H., 2016. U-Pb dating of detrital zircons of metamorphic sandstone from Dongnancha formation in the Hudian area of Jilin Province. *China Science paper*, 11(9): 995–1004 (in Chinese with English abstract).

Heard, H.C., and Raleich, C.B., 1972. Steady-state flow in marble at 500° to 800 °C. *Geological Society of*

America Bulletin, 83: 935–956.

Herwegh, M., and Handy, M.R., 1998. The origin of shape preferred orientations in mylonite: inference from in-situ experiments on polycrystalline norcamphor. *Journal of Structural Geology*, 20: 681–694.

Herwegh, M., and Pfiffner, O.A., 2005. Tectono-metamorphic evolution of a nappe stack: a case study of the Swiss Alps. *Tectonophysics*, 404: 55–76.

Herwegh, M., de Bresser, J.H.P., and ter Heege, J.H., 2005. Combining natural microstructures with composite flow laws: an improved approach for the extrapolation of lab data to nature. *Journal of Structural Geology*, 27: 503–521.

Heumann, M.J., Johnson, C.L., Webb, L.E., Taylor, J.P., and Minjin, C., 2014. Total and incremental left-lateral displacement across the East Gobi Fault Zone, southern Mongolia: Implications for timing and modes of polyphase intracontinental deformation. *Earth and Planetary Science Letters*, 392: 1–15.

Hirth, G., and Tullis, J., 1992. Dislocation creep regimes in quartz aggregates. *Journal of Structural Geology*, 14: 145–159.

Hirth, G., Teyssier, C., and Dunlap, W.J., 2001. An evaluation of quarzite flow laws based on comparisons between experimentally and naturally deformed rocks. *International Journal Of Earth Sciences*, 90: 77–87.

Holyoke, C.W., and Tullis, J., 2006. Formation and maintenance of shear zones. *Geology*, 34: 105–108.

Holyoke, C.W., Kronenberg, A.K., and Newman, J., 2013. Dislocation creep of polycrystalline dolomite. *Tectonophysics*, 590: 72–82.

Hong, X., Peng, X.L., Liu, L., Qu, X.Y., Li, F.L., and Yang, D.M., 2009. Characteristics of the Dark Marine Mudstone of the Lower Carboniferous Luquantun Formation in the Panshi Area, Central Jilin Province. *Journal of Jilin University (*Earth Science Edition*)*, 39(2): 225–231 (in Chinese with English abstract).

IMBGMR (Inner Mongolian Bureau of Geology and Mineral Resources), 1991. Regional Geology of Inner Mongolian Autonomous Region. *Geological Publishing House, Beijing*, 1–725 (in Chinese with English abstract).

Jahn, B.M., 2004. The central Asian orogenic belt and growth of the continental crust in the phanerozoic. *Geological Society of London, Special Publications*, 226: 73–100.

JBGMR (Jilin Bureau of Geology and Mineral Resources), 1988. Regional Geology of Jilin Province. *Geological Publishing House, Beijing*, 12–698 (in Chinese with English summary).

JBGMR (Jilin Bureau of Geology and Mineral Resources), 1997. Lithostratigraphy of Jilin Province. *China University of Geosciences Press, Wuhan*, 1–324 (in Chinese).

Jia, D.C., Hu, R.Z., Lu, Y., and Qiu, X.L., 2004. Collision belt between the Khanka block and the North China block in the Yanbian Region, Northeast China. *Journal of Asian Earth Sciences*, 23: 211–219.

Jian, P., Liu, D.Y., Kröner, A.,Windley, B.F., Shi, Y.Y., Zhang, F.Q., Shi, G.H., Miao, L.C., Zhang, W., Zhang, Q., Zhang, L.Q., and Ren, J.S., 2008. Time scale of an early to mid-Paleozoic orogenic cycle of the long-lived Central Asian Orogenic Belt, Inner Mongolia of China: Implications for continental growth. *Lithos*, 101: 233–259.

Johnson, C.L., 2004. Polyphase evolution of the East Gobi basin: sedimentary and structural records of Mesozoic-Cenozoic intraplate deformation in Mongolia. *Basin Research*, 16: 79–99.

Kennedy, L.A., and White, J.C., 2001. Low-temperature recrystallization in calcite: mechanisms and consequences. *Geology*, 29: 1027–1030.

Kollmeier, J.M., van der Pluijm, B.A., and Van der Voo, R., 2000. Analysis of Variscan dynamics; early bending of the Cantabria-Asturias Arc, northern Spain. *Earth and Planetary Science Letters*, 181: 203–216.

Kröner, A., Kovach, V., Alexeiev, D., Wang, K.L., Wong, J., Degtyarev, K., and Kozakov, I., 2017. No excessive crustal growth in the Central Asian Orogenic Belt: Further evidence from field relationships and isotopic data. *Gondwana Research*, 50: 135–166.

Kröner, A., Kovach, V., Belousova, E., Hegner, E., Armstrong, R., Dolgopolova, A., Seltmann, R., Alexeiev, D.V., Hoffmann, J.E., Wong, J., Sun, M., Cai, K., Wang, T., Tong, Y., Wilde, S.A., Degtyarev, K.E., and Rytsk, E., 2014. Reassessment of continental growth during the accretionary history of the Central Asian Orogenic Belt. *Gondwana Research*, 25: 103–125.

Kruhl, J.H., 1996. Prism- and basal-plane parallel subgrain boundaries in quartz: a microstructural geothermobarometer. *Journal Of Metamorphic Geology*, 14: 581–589.

Kruhl, J.H., and Nega, M., 1996. The fractal shape of sutured quartz grain boundaries: application as a geothermometer. *International Journal of Earth Sciences*, 85(1): 38–43.

Kruhl, J.H., Nega, M., and Milla, H.E., 1995. The fractal shape of grain boundary sutures: reality, model and application as a geothermometer. *Book of Abstracts, 2nd Int. Conference Fractal and Dynamic Systems in Geosciences*, 84: 31–32.

Kruse, R., Stünitz, H., and Kunze, K., 2001. Dynamic recrystallization processes in plagioclase porphyroclasts. *Journal of Structural Geology*, 23: 1781–102.

Lacombe, O., 2007. Comparison of paleostress magnitudes from calcite twins with contemporary stress magnitudes and frictional sliding criteria in the continental crust: Mechanical implications. *Journal of Structural Geology*, 29: 86–99.

LaFrance, B., White, J.C., and Williams, P.F., 1994. Natural calcite c-axis fabrics: an alternative explanation. *Tectonophysics*, 229: 1–18.

Lamb, M.A., Hanson, A.D., Graham, S.A., Badarch, G., and Webb, L.E., 1999. Left-lateral sense offset of Upper Proterozoic to Paleozoic features across the Gobi Onon, Tost, and Zuunbayan faults in southern Mongolia and implications for other central Asian faults. *Earth and Planetary Science Letters*, 173: 183–194.

Laurent, P., Kern, H., and Lacombe, O., 2000. Determination of deviatoric stress tensors based on inversion of calcite twin data from experimentally deformed monophase samples. Part II. Axial and triaxial stress experiments. *Tectonophysics*, 327: 131–148.

Law, R.D., Searle, M.P., and Simpson, R.L., 2004. Strain, deformation temperatures and vorticity of flow at the top of the Greater Himalayan slab, Everest massif, Tibet. *Journal of The Geological Society*, 161: 305–320.

Leiss, B., Siegesmund, S., and Weber, K., 1999. Texture asymmetries as shear sense indicators in naturally deformed mono- and polyphase carbonate rocks. *Textures and Microstructures*, 33: 61–74.

Li, C.D., Zhang, F.Q., Miao, L.C., Xie, H.Q., and Xu, Y.W., 2007. Zircon SHRIMP geochemistry of late Permian high-Mg andesites in Seluohe area, Jilin Province, China. *Acta Petrologica Sinica*, 23 (4): 767–776 (in Chinese with English abstract).

Li, D.P., Jin, Y., Hou, K.J., Chen, Y.L., and Lu, Z., 2015. Late Paleozoic final closure of the Paleo-Asian Ocean in the eastern part of the Xing-Meng Orogenic Belt: Constraints from Carboniferous-Permian (meta-) sedimentary strata and (meta-) igneous rocks. *Tectonophysics*, 665: 251–262.

Li, J.B., Wang, T., and Ouyang, Z. X., 2010. Strain and kinematic vorticity analysis of the Louzidian low-angle ductile shear detachment zone in Chifeng, Inner Mongolia, China. *Science in China (*Earth Sciences*)*, 53: 1611–1624.

Li, J.Y., 2006. Permian geodynamic setting of Northeast China and adjacent regions: closure of the Paleo-Asian Ocean and subduction of the Paleo-Pacific Plate. *Journal of Asian Earth Sciences*, 26 (3–4): 207–224.

Li, S.Z., Suo, Y.H., Li, X.Y., Zhou, J, Santosh, M, Wang, P.C., Wang, G.Z., Guo, L.L., Yu, S.Y., Lan, H.Y., Dai, L.M., Zhou, Z.Z., Gao, X.Z., Zhou, J.J.., Liu, B, Jiang, S.H., Wang, G, and Zhang, G.W., 2019. Mesozoic tectono-magmatic response in the East Asian ocean-continent connection zone to subduction of the Paleo-Pacific Plate. *Earth-Science Reviews*, 192: 91–137.

Li, Y.L., Brouwer, F.M., Xiao, W.J., Wang, K.L., Lee, Y.H., Luo, B.J., Su, Y.P., and Zheng, J.P., 2017. Subduction-related metasomatic mantle source in the eastern Central Asian Orogenic Belt: Evidence from amphibolites in the Xilingol Complex, Inner Mongolia, China. *Gondwana Research*, 43: 193–212.

Li, Y.L., Zhou, H.W., Brouwer, F.M., Xiao,W.J., Wijbrans, J.R., Zhao, J.H., Zhong, Z.Q., and Liu, H.F., 2014. Nature and timing of the Solonker suture of the Central Asian Orogenic Belt: insights from geochronology and geochemistry of basic intrusions in the Xilin Gol Complex, Inner Mongolia, China. *International Journal of Earth Sciences*, 103: 41–60.

Liang, C., Liu, Y., Neubauer, F., Bernroider, M., Jin, W., Li, W., Zeng, Z., Wen, Q., and Zhao, Y., 2015. Structures, kinematic analysis, rheological parameters and temperature-pressure estimate of the Mesozoic Xingcheng-Taili ductile shear zone in the North China Craton. *Journal of Structural Geology*, 78: 27–51.

Liang, C.Y., Liu, Y.J., Li, W., Han, G.Q., Wen, Q.B., and Zhao, Y.L., 2011. Characteristics of extensional structure of Keluo complex in Nenjiang area, Heilongjiang, China. *Geological Bulletin of China*, 30(2–3): 291–299 (in Chinese with English abstract).

Liang, C.Y., Liu, Y.J., Zheng, C.Q., Li, W.M., Neubauer, F., Zhang, Q., and Zhang, D., 2019. Deformation patterns and timing of the thrust- nappe structures in the Mohe Formation in Mohe Basin, Northeast China: Implication of the closure timing of Mongol-Okhotsk ocean. *Geological Journal*, 54: 746–769.

Liang, C.Y., Liu, Y.J., Zhu, J.J., Li, W.M., Chang, R.H., and Zhang, L., 2017. Deformation Fabrics and Rheological Features of Early Permian Fanjiatun Formation from Quannongshan Area, Southeastern Changchun. *Earth Science*, 42(12): 2174–2192 (In Chinese with English abstract).

Lister, G.S., 1977. Discussion: Crossed girdle c-axis fabrics in quartzites plastically deformed by plane strain and progressive simple shear. *Tectonophysics*, 39: 51–54.

Liu, D., Jian, P., Kroner, A., and Xu, S., 2006. Dating of prograde metamorphic events deciphered from episodic zircon growth in rocks of the Dabie-Sulu UHP complex, China. *Earth and Planetary Science Letters*, 250: 650–666.

Liu, J., Tang, Y., Tran, M.D., Cao, S., Zhao, L., Zhang, Z., and Chen, W., 2012. The nature of the Ailao Shan-Red River (ASRR) shear zone: Constraints from structural, microstructural and fabric analyses of metamorphic rocks from the Diancang Shan, Ailao Shan and Day Nui Con Voi massifs. *Journal of Asian Earth Sciences*, 47: 231–251.

Liu, J.L., Cao, S.Y., Zou, Y.X., and Song, Z.J., 2008. EBSD analysis of rock fabrics and its application. *Geological Bulletin of China*, 27: 1638–1645 (in Chinese with English abstract).

Liu, Y.J., Li, W.M., Feng, Z.Q., Wen, Q.B., Neubauer, F., and Liang, C.Y., 2017. A review of the Paleozoic tectonics in the eastern part of Central Asian Orogenic Belt. *Gondwana Research*, 43: 123–148.

Liu, Y.J., Zhang, X.Z., Jin,W., Chi, X.G.,Wang, C.W., Ma, Z.H., Han, G.Q.,Wen, Q.B., Li,W., Wang, W.D., and Zhao, X.F., 2010. Late Paleozoic tectonic evolution in Northeast China. *Geology in China*, 37: 943–951 (in Chinese with English abstract).

Llana-Fúnez, S., and Rutter, E.H., 2008. Strain localization in direct shear experiments on Solnhofen limestone at high temperature-effects of transpression. *Journal of Structural Geology*, 30: 1372–1382.

Ma, A., 2009. $^{40}Ar/^{39}Ar$ dating of muscovite in mylonite of Shang Gang Gang Kun Dui Fault. New evidence for the main stage of Xar Moron River Fault zone. *Xinjiang Geology*, 27: 170–175 (in Chinese with English abstract).

Ma, X., Chen, B., Chen, J.F., and Niu, X.L., 2013. Zircon SHRIMP U-Pb age, geochemical, Sr-Nd isotopic, and in-situ Hf isotopic data of the Late Carboniferous-Early Permian plutons in the northern margin of the North China Craton. *Science China Earth Sciences*, 56: 126–144.

Marques, F.O., Machek, M., Roxerová, Z., Burg, J.P., and Almqvist, B.S.G., 2015. Mechanics, microstructure and AMS evolution of a synthetic porphyritic calcite aggregate deformed in torsion. *Tectonophysics*, 655: 41–57.

Means, W.D., 1994. Rotational quantities in homogeneous flow and the development of small scale structure. *Journal of Structural Geology*, 16: 437–445.

Means, W.D., 1995. Shear zones and rock history. *Tectonophysics*, 247: 157–160.

Means, W.D., Hobbs, B.E., and Lister, G.S., 1980. Vorticity and non-coaxiality in progressive deformation. *Journal of Structural Geology*, 2: 371–378.

Meng, Q.R., 2003. What drove late Mesozoic extension of the northern China-Mongolia tract? *Tectonophysics*, 369: 155–174.

Meng, Q.R., and Zhang, G.W., 1999. Timing of collision of the North and South China blocks: controversy and reconciliation. *Geology*, 27: 123–126.

Michel, B., David, J. P., and Bernhard, G., 2006. Characterisation of deformation and flow mechanics around porphyroclasts in a calcite marble ultramylonite by means of EBSD analysis. *Tectonophysics*, 413: 185–200.

Molli, G., Conti, P., Giorgetti, G., Meccheri, M., and Oesterling, N., 2000. Microfabric study on the deformational and thermal history of the Alpi Apuane marbles (Carrara marbles), Italy. *Journal of Structural Geology*, 22: 1809–1825.

Molli, G., White, J.C., Kennedy, L., and Taini, V., 2011. Low-temperature deformation of limestone, Isola Palmaria, northern Apennine, Italy-The role of primary textures, precursory veins and intracrystalline deformation in localization. *Journal of Structural Geology*, 33: 255–270.

Montési, L.G.J., and Hirth, G., 2003. Grain size evolution and the rheology of ductile shear zones: from laboratory experiments to postseismic creep. *Earth and Planetary Science Letters*, 211: 97–110.

Negrini, M., Smith, S.A.F., Scott, J.M., and Tarling, M.S., 2018. Microstructural and rheological evolution of calcite mylonites during shear zone thinning: Constraints from the Mount Irene shear zone, Fiordland, New Zealand. *Journal of Structural Geology*, 106: 86–102.

Newman, J., 1994. The influence of grain size and grain size distribution on methods for estimating paleostresses from twinning in carbonates. J*ournal of Structural Geology*, 16: 1589–1601.

Nozaka, T., and Liu, Y., 2002. Petrology of the Hegenshan ophiolite and its implications for the tectonic evolution of northern China. *Earth and Planetary Science Letters*, 202: 89–104.

Oesterling, N., Heilbronner, R., Stünitz, H., Barnhoorn, A., and Molli, G., 2007. Strain dependent variation of

microstructure and texture in naturally deformed Carrara marble. *Journal of Structural Geology*, 29: 681–696.

Okudaira, T., and Shigematsu, N., 2012. Estimates of stress and strain rate in mylonites based on the boundary between the fields of grain-size sensitive and insensitive creep. *Journal of Geophysical Research: Solid Earth*, 11: B03210.

Parlangeau, C., Lacombe, O., Schueller, S., and Daniel, J.M., 2018. Inversion of calcite twin data for paleostress orientations and magnitudes: A new technique tested and calibrated on numerically-generated and natural data. *Tectonophysics*, 722: 462–485.

Passchier, C.W., 1987. Stable position of rigid objects in non-coaxial flow-a study in vorticity analysis. *Journal of Structural Geology*, 9: 670–69.

Passchier, C.W., 1998. Monoclinic model shear zones. *Journal of Structural Geology*, 20: 1121–1137.

Passchier, C.W., and Urai, J.L., 1988. Vorticity and strain analysis using Mohr diagrams. *Journal of Structural Geology*, 10: 755–763.

Passchier, C.W., Simpson, C., 1986. Porphyroclast systems as kinematic indicators. *Journal of Structural Geology*, 8: 895–910.

Paterson, M.S., and Luan, F.C., 1990. Quartzite rheology under geological conditions. *Geological Society, London, Special Publications*, 54(1): 299–307.

Pfiffner, O.A., and Ramsay, J.G., 1982. Constraints on geological strain rates: arguments from finite strain rates of naturally deformed rocks. *Journal of Geophysical Research*, 87: 311–321.

Pieri, M., Burlini, L., Kunze, K., Stretton, I., and Olgaard, D.L., 2001. Rheological and microstructural evolution of Carrara marble with high shear strain; results from high temperature torsion experiments. *Journal of Structural Geology*, 23:1393–1413.

Poirier, J., 1985. Creep of Crystals: High-temperature Deformation Processes in Metals, Ceramics and Minerals. *Cambridge University Press*, *Cambridge*, 1-260.

Poirier, J.P., 1980. Shear localization and shear instability in materials in the ductile field. *Journal of Structural Geology*, 2: 135–142.

Ramsay, J.G., 1980. Shear zone geometry: a review. *Journal of Structural Geology*, 2: 83–89.

Ree, J.H., 1991. An experimental steady-state foliation. *Journal of Structural Geology,* 13: 1001–1011.

Renner, J., Evans, B., and Siddiqi, G., 2002. Dislocation creep of calcite. *Journal of Geophysical Research*, 107: 1–16.

Reston, T. J., 1990. The lower crust and the extension of the continental lithosphere: kinematic analysis of BIRPS deep seismic data, *Tectonics*, 9: 1235–1248.

Rocher, M., Cushing, M., Lemeille, F., Lozach, Y., and Angelier, J., 2004. Intraplate paleostresses reconstructed with calcite twinning and faulting: improved method and application to the eastern Paris Basin (Lorraine, France). *Tectonophysics*, 387: 1–21.

Rogowitz, A., White, J.C., and Grasemann, B., 2016. Strain localization in ultramylonitic marbles by simultaneous activation of dislocation motion and grain boundary sliding (Syros, Greece). *Solid Earth*, 7(2): 355–366.

Rowe, K.J., and Rutter, E.H., 1990. Palaeostress estimation using calcite twinning: experimental calibration and application to nature. *Journal of Structural Geology*, 12: 1–17.

Rowley, D.B., Xue, F., Tucker, R.D., Peng, Z.X., Baker, J., and Davis, A., 1997. Ages of ultrahigh pressure metamorphism and protolith orthogneisses from the eastern Dabie Shan: U-Pb zircon geochronology. *Earth and Planetary Science Letters*, 151: 191–203.

Rutter, E.H., 1972. Influence of interstitial water on rheological behavior of calcite rocks. *Tectonophysics*, 14: 13–33.

Rutter, E.H., 1974. Influence of temperature, strain rate and interstitial water in experimental deformation of calcite rocks. *Tectonophysics*, 22, 311–334.

Rutter, E.H., 1995. Experimental study of the influence of stress, temperature, and strain on the dynamic recrystallization of Carrara marble. *Journal of Geophysical Research : Solid Earth*, 100(B12): 24651–24663.

Rutter, E.H., and Brodie, K.H., 1988. The role of tectonic grain size reduction in the rheological stratification of the lithosphere. *Geologische Rundschau*, 77: 295–307.

Rutter, E.H., and Brodie, K.H., 2004a. Experimental grain-size sensitive flow of hot-pressed Brazilian quartz aggregates. *Journal of Structural Geology*, 26: 2011–2023.

Rutter, E.H., and Brodie, K.H., 2004b. Experimental intracrystalline plastic flow in hot-pressed synthetic quartzite prepared from Brazilan quartz crystals. *Journal of Structural Geology*, 26: 259–270.

Rutter, E.H., Casey, M., and Burlini, L., 1994. Preferred crystallographic orientation development during the plastic and superplastic flow of calcite rocks. *Journal of Structural Geology*, 10: 1431–1446.

Safonova, I., 2017. Juvenile versus recycled crust in the Central Asian Orogenic Belt: Implications from ocean plate stratigraphy, blueschist belts and intra-oceanic arcs. *Gondwana Research*, 47: 6–27.

Safonova, I.Yu., and Santosh, M., 2014. Accretionary complexes in the Asia-Pacific region: tracing archives of ocean plate stratigraphy and tracking mantle plumes. *Gondwana Research*, 25: 126–158.

Safonova, I.Yu., Seltmann, R., Kröner, A., Gladkochub, D., Schulmann, K., Xiao, W.J., Kim, J.Y., Komiya, T., and Sun, M., 2011. A new concept of continental construction in the Central Asian Orogenic Belt. *Episodes*, 34: 186–196.

Schmalholz, S.M., and Duretz, T., 2017. Impact of grain size evolution on necking in calcite layers deforming by combined diffusion and dislocation creep. *Journal of Structural Geology*, 103: 37–56.

Schmid S.M., J.N. Boland, and Paterson, M.S., 1977. Superplastic flow in fine-grained limestone, *Tectonophysics*, 43: 257–291.

Schmid, S.M., and Casey, M., 1986. Complete fabric analysis of some commonly observed quartz C-axis patterns. *Geophysical Monogrographs*, 36: 263–286.

Schmid, S.M., Panozzo, R., and Bauer, S., 1987. Simple shear experiments on calcite rocks: rheology and microfabric. *Journal of Structural Geology*, 9: 747–778.

Schmid, S.M., Paterson, M.S., and Boland, J.N., 1980. High temperature flow and dynamic recrystallization in carrara marble. *Tectonophysics*, 65(3): 245–280.

Sengör, A.M.C., Natal'in, B.A., and Burtman, U.S., 1993. Evolution of the Altaid tectonic collage and Paleozoic crustal growth in Eurasia. *Nature*, 364: 209–304.

Sibson, R.H., 1977. Fault rocks and fault mechanisms. *Journal of the Geological Society of London*, 133: 191–213.

Siddans, A.W., Henry, B., and Kligfield, R., 1984. Finite strain patterns and their significance in Permian rocks of the Alpes Maritimes (France). *Journal of Structural Geology*, 6: 339–368.

Simpson, C., and De Paor, D.G., 1993. Strain and kinematic analysis in general shear zones. *Journal of Structural Geology*, 15: 1–20.

Song, Z.G., Han, Z.Z., Gao, L.H., Geng, H.Y., Li, X.P., Meng, F.X., Han, M., Zhong, W.J., Li, J.J., Du, Q.X., Yan, J.L., and Liu, H., 2018. Permo-Triassic evolution of the southern margin of the Central Asian Orogenic Belt revisited: Insights from Late Permian igneous suite in the Daheishan Horst, NE China. *Gondwana Research*, 56: 23–50.

Spanos, D., Xypolias, P., and Koukouvelas, I., 2015. Vorticity analysis in calcite tectonites: An example from the Attico-Cycladic massif (Attica, Greece). *Journal of Structural Geology*, 80: 120–132.

Stipp, M., Tullis, J., and Scherwath, M., 2010. A new perspective on paleo-piezometry: Dynamically recrystallized grain size distributions indicate mechanism changes. *Geology*, 38(8): 759–762.

Stone, D., and Schwerdtner, W.M., 1981. Total strain within a major mylonite zone, southern Canadian Shield. *Journal of Structural Geology*, 3: 193–194.

Sun, D.Y., Wu, F.Y., Zhang, Y.B., and Gao, S., 2004. The final closing time of the west Lamulun River-Changchun-Yanji plate suture zone: evidence from the Dayushan granitic pluton, Jilin Province. *Journal of Jilin University (Earth Science Edition)*, 34(2): 174–181 (in Chinese with English abstract).

Sun, Y., Li, M., Ge, W., Zhang, Y., and Zhang, D., 2013. Eastward termination of the Solonker-Xar Moron River Suture determined by detrital zircon U-Pb isotopic dating and Permian floristics. *Journal of Asian Earth Sciences*, 75: 243–250.

Takahashi, M., Nagahama, H., and Masuda, T., 1998. Fractal analysis of experimentally, dynamically recrystallized quartz grains and its possible application as a strain rate meter. *Journal of Structural Geology*, 20(2–3): 269–275.

Tang, K., 1990. Tectonic development of Paleozoic fold belts at the north margin of the Sino-Korean craton. *Tectonics*, 9: 249–260.

Tikoff, B., and Fossen, H., 1995. The limitations of three-dimensional kinematic vorticity analysis. *Journal of Structural Geology*, 17(12): 1771–1784.

Tikoff, B., and Fossen, H., 1999. Three-dimensional reference deformations and strain facies. *Journal of Structural Geology*, 21: 1497–1512.

Tikoff, B., and Greene, D., 1997. Stretching lineations in transpressional shear zones. *Journal of Structural Geology*, 19: 29–40.

Tripathy, V., and Saha, D., 2015. Inversion of calcite twin data, paleostress reconstruction and multiphase weak deformation in cratonic interior-Evidence from the Proterozoic Cuddapah basin, India. *Journal of Structural Geology*, 77: 62–81.

Trullenque, G., Kunze, K., Heilbronner, R., Stünitz, H., and Schmid, M.S., 2006. Microfabrics of calcite ultramylonites as records of coaxial andnon-coaxial deformation kinematics: examples from the Rocher de l'Yret shear zone (Western Alps). *Tectonophysics*, 424: 69–97.

Twiss, R. J., 1977. Theory and applicability of a recrystallized grain size paleopiezometer. *Pure and Applied Geophysics*, 115(1): 227–244.

Ulrich, S., Schulmann, K., and Casey, M., 2002. Microstructural evolution and rheological behavior of marbles deformed at different crustal levels. *Journal of Structural Geology*, 24: 979–995.

Van der Pluijm, B.A., 1991. Marble mylonites in the Bancroft shear zone, Ontario, Canada: microstructures and deformation mechanisms. *Journal of Structural Geology*, 13: 1125–1135.

Vernon, R. H, 1981. Optical microstructure of partly recrystallized calcite in some naturally deformed marbles. *Tectonophysics*, 78(1–4): 601–612.

Voll, G., 1976. Recrystallization of quartz, biotite and feldspars from Erstfeld to the Leventina Nappe, Swiss Alps, and its geological significance. *Schweizer Mineralogische und Petrographische Mitteilungen*, 56: 641–647.

Walker, A.N., Rutter, E.H., and Brodie, K.H., 1990. Experimental Study of Grain-size Sensitive Flow of Synthetic, Hot-pressed Calcite Rocks, Deformation Mechanisms, Rheology and Tectonics. *Geological Society of London, London, United Kingdom*, 259–284.

Wallis, S.R., 1995. Vorticity analysis and recognition of ductile extension in the Sanbagawa belt, SW Japan. *Journal of Structural Geology*, 17: 1077–1093.

Wang, B., Zhou, J.B., Wilde, S.A., Zhang, X.Z., Ren, S.M., 2016. The timing of final closure along the Changchun-Yanji suture zone: Constraints fromdetrital zircon U-Pb dating of the Triassic Dajianggang Formation, NE China. *Lithos*, 261: 216–231.

Wang, F., Xu,W.L., Gao, F.H., Zhang, H.H., Pei, F.P., Zhao, L., and Yang, Y., 2013. Precambrian terrane within the Songnen-Zhangguangcai Range Massif, NE China: evidence from U-Pb ages of detrital zircons fromthe Dongfengshan and Tadong groups. *Gondwana Research*, 26: 402–413.

Wang, G.S., Wu, C., Chen, C., Zhou, Z.G., Liu, C.F., and Jiang, T., 2017. Geochronological data of igneous and metamorphic rocks from the Xing'an-Mongolia Orogenic Belt of the eastern Central Asian Orogenic Belt: implications for the fnal closure of the Paleo- Asian Ocean. *International Journal of Earth Sciences*, 106: 2727–2746.

Wang, X.S., Zheng, Y.D., and Wang, T., 2007. Strain and shear types of the Louzidian ductile shear zone in southern Chifeng, Inner Mongolia, China. *Science in China(Earth Sciences)*, 50: 487–495.

Wang, X.S., Zheng, Y.D., and Zhang, J.J., 2002. Extensional kinematics and shear type of the Hohhot metamorphic core complex, Inner Mongolia. *Geological Bulletin of China*, 21: 238–243 (in Chinese with English abstract).

Wang, Y.B., Liang, M.H., and Huo, Q.Z., 2004. The study of limit deformation measurement with deformation feldspar in granite areas. *Northwest Geology*, 37(1): 19–24 (in Chinese with English abstract).

Wang, Y.S., Xiang, B.W., Zhu, G., and Jiang, D.Z., 2011. Structural andgeochronological evidence for Early Cretaceous orogen- parallelextension of the ductile lithosphere in the northern Dabie orogenicbelt, East China. *Journal of Structural Geology*, 33: 362–380.

Wang, Z.J., Xu, W.L., Pei, F.P.,Wang, Z.W., Li, Y., and Cao, H.H., 2015. Geochronology and geochemistry of middle Permian-Middle Triassic intrusive rocks from central-eastern Jilin Province, NE China: Constraints on the tectonic evolution of the eastern segment of the Paleo-Asian Ocean. *Lithos*, 238: 13–25.

Webb, L.E., and Johnson, C.L., 2006. Tertiary strike-slip faulting in southeastern Mongolia and implications for Asian tectonics. *Earth and Planetary Science Letters*, 241: 323–335.

Webb, L.E., Johnson, C.L., and Minjin, C., 2010. Late Triassic sinistral shear in the East Gobi Fault Zone, Mongolia. *Tectonophysics*, 495: 246–255.

Weijermars, R., 1991. The role of stress in ductile deformation. *Journal of Structural Geology*, 13: 1061–1078.

Weijermars, R., 1993. Progressive deformation of single layers under constantly oriented boundary stresses.

Journal of Structural Geology, 15: 911–922.

Weijermars, R., 1998. Taylor-mill analogues for patterns of flow and deformation in rocks. *Journal of Structural Geology*, 20: 77–92.

Wenk, H.R., Takeshita, T., Bechler, E., Erskine, B.G., and Matthies, S., 1987. Pure shear and simple shear calcite textures. Comparison of experimental, theoretical and natural data. *Journal of Structural Geology*, 9: 731–745.

Wernicke, B., 1985. Uniform sense simple shear of the continental lithosphere. *Canadian Journal of Earth Sciences*, 22: 108–125.

Wheeler, J., Prior, D.J., Jiang, Z., Spiess, R., and Trimby, P.W., 2001. The petrological significance of misorientations between grains. *Contributions to Mineralogy and Petrology*, 141: 109–124.

White, S., 1979. Grain and sub-grain size variation across a mylonite zone. *Contributions to Mineralogy and Petrology*, 70: 193–202.

Wilde, S.A., 2015. Final amalgamation of the Central Asian Orogenic Belt in NE China: Paleo-Asian Ocean closure versus Paleo-Pacific plate subduction-A review of the evidence. *Tectonophysics*, 662: 345–362.

Wilde, S.A., and Zhou, J.B., 2015. The late Paleozoic to Mesozoic evolution of the eastern margin of the Central Asian Orogenic Belt in China. *Journal of Asian Earth Sciences*, 113: 909–921.

Wilde, S.A., Wu, F.Y., and Zhang, X.Z., 2003. Late Pan-African magmatism in Northeastern China: SHRIMP U-Pb zircon evidence for igneous ages from the Mashan Complex. *Precambrian Research*, 122: 311–327.

Wilde, S.A., Zhang, X.Z.,and Wu, F.Y., 2000. Extension of a newly identified 500 Ma metamorphic terrane in North East China: further U-Pb SHRIMP dating of the Mashan Complex, Heilongjiang Province, China. *Tectonophysics*, 328: 115–130.

Windley, B.F., Alexeiev, D., Xiao, W., Kröner, A., and Badarch, G., 2007. Tectonic models for accretion of the Central Asian Orogenic belt. *Journal of the Geological Society*, 164: 31–47.

Wu, F.Y., Lin, J., Wilde, S.A., Zhang, X.O., and Yang, J., 2005. Nature and significance of the Early Cretaceous giant igneous event in eastern China. *Earth and Planetary Science Letters*, 233: 103–119.

Wu, F.Y., Sun, D.Y., Ge, W.C., Zhang, Y.B., Grant, M.L., Wilde, S.A., and Jahn, B.M., 2011. Geochronology of the Phanerozoic granitoids in northeastern China. *Journal of Asian Earth Sciences*, 41: 1–30.

Wu, S.P., Wang, M.Y., and Qi, K.J., 2007. Present situation of researches on A-type granites: a review. *Acta Petrologica et Mineralogica*, 26: 57–66 (in Chinese with English abstract).

Xia, H.R. and Liu, J.L., 2011. The crystallographic preferred orientation of quartz and its applications. *Geological Bulletin of China*, 30(1): 58–70 (in Chinese with English abstract).

Xiao, W.J., and Santosh, M., 2014. The western Central Asian Orogenic Belt: A window to accretionary orogenesis and continental growth. *Gondwana Research*, 25: 1429–1444.

Xiao, W.J., Windley, B., Hao, J., and Zhai, M.G., 2003. Accretion leading to collision and the Permian Solonker suture, Inner Mongolia, China: termination of the Central Asian Orogenic Belt. *Tectonics*, 22: 1069–1089.

Xiao,W.J.,Windley, B.F., Sun, S., Li, J.L., Huang, B.C., Han, C.M., Yuan, C., Sun, M., and Chen, H.L., 2015. A tale of amalgamation of three Permo-Triassic collage systems in Central Asia: oroclines, sutures, and terminal accretion. *Annual Review of Earth and Planetary Sciences*, 43: 477–507.

Xu, B., Charvet, J., Chen, Y., Zhao, P., and Shi, G., 2013. Middle Paleozoic conver-gent orogenic belts in western Inner Mongolia (China): framework, kinematics, geochronology and implications for tectonic evolution of the Central Asian Orogenic Belt. *Gondwana Research*, 23: 1342–1364.

Xu, B., Zhao, P., Wang, Y.Y., Liao, W., Luo, Z.W., Bao, Q.Z., and Zhou, Y.H., 2015. The pre-Devonian tectonic framework of Xing'an-Mongolia orogenic belt (XMOB) in north China. *Journal of Asian Earth Sciences*, 97: 183–196.

Xu, Y.G., Li, H.Y., Pang, C.J., and He, B., 2009a. On the timing and duration of the destruction of the North China craton. *Chinese Science Bulletin*, 54: 3379–3396.

Xu, Z.Q., Wang, Q., Liang, F.H., Chen, F.Y., and Xu, C.P., 2009b. Electron backscatter diffracion (EBSD) technique and its application to study of continental dynamic. *Acta Petrologica Sinica*, 25(7): 1721–1736 (in Chinese with English abstract).

Xypolias, P., 2009. Some new aspects of kinematic vorticity analysis in naturally deformed quartzites. *Journal of Structural Geology*, 31: 3–10.

Xypolias, P., 2010. Vorticity analysis in shear zones: a review of methods and applications. *Journal of Structural Geology*, 32: 2072–2092.

Xypolias, P., and Doutsos, T., 2001. Kinematic vorticity and strain rate patterns associated with ductile extrusion in the Chelmos Shear Zone External Hellenides, Greece. *Tectonophysics*, 338: 59–77.

Xypolias, P., Chatzaras, V., Beane, R., and Papadopoulou, S., 2013. Heterogeneous constrictional deformation in a ductile shear zone resulting from the transposition of a lineation-parallel fold. *Journal of Structural Geology*, 52: 44–59.

Yang, X.Y., 2005. On the studies of ductile shear zone: their geological significance. *Advances in Earth science*, 20(7): 765–771 (in Chinese with English abstract).

Yu, S.Y., Li, S.Z., Zhang, J.X., Peng Y.B., Somerville, I., Liu Y.J., Wang Z.Y., Li, Z.F., Yao, Y., and Li, Y., 2019a. Multistage anatexis during tectonic evolution from oceanic subduction to continental collision: A review of the North Qaidam UHP Belt, NW China. *Earth-Science Reviews*, 191: 190–211.

Yu, S.Y., Li, S.Z., Zhang, J.X., Sun, D.Y., and Peng, Y.B., 2018. Linking high-pressure mafic granulite, TTG-like (tonalitic-trondhjemitic) leucosome and pluton, and crustal growth during continental collision. *Geological Society of American Bulletin*, 131(3–4): 572–586.

Yu, S.Y., Zhang, J.X., Li, S.Z., Santosh, M., Li, Y.S., Liu, Y.J., Li, X.Y., Peng, Y.B., Sun, D.Y., Wang, Z.Y., and Lv, P., 2019b. TTG-Adakitic-Like (Tonalitic-Trondhjemitic) Magmas Resulting From Partial Melting of Metagabbro Under High-Pressure Condition During Continental Collision in the North Qaidam UHP Terrane, Western China. *Tectonics*, 38(3): 791–822.

Zhai, M.G., Zhu, R.X., and Liu, J.M., 2004. Time-range of Mesozoic tectonic regime inversion in eastern China block. *Science in China (Earth Sciences)*, 47: 151–160.

Zhang, B., Chai, Z., Yin, C.Y., Huang, W.T., Wang, Y., Zhang, J.J., and Cao, K., 2017. Intra-continental transpression and gneiss doming in an obliquely convergent regime in SE Asia. *Journal of Structural Geology*, 97: 48–70.

Zhang, B., Zhang, J., Liu, J., Wang, Y., Yin, C., Guo, L., and Yue, Y., 2014. The Xuelongshan high strain zone: Cenozoic structural evolution and implications for fault linkages and deformation along the Ailao Shan-Red River shear zone. *Journal of Structural Geology*, 69: 209–233.

Zhang, B., Zhang, J.J., and Guo, L., 2006. Analysis of structural features and deformation of the mylonite zone in the detachment fault system of the Yalaxiangbo metamorphic complex core, Northern Himalayan Dome belt. *Progress in Natural Science*, 15(6): 692–699 (in Chinese with English abstract).

Zhang, J., Li, J.Y., Xiao, W.X., Wang, Y.N., and Qi, W.H. 2013. Kinematics and geochronology of multistage ductile deformation along the eastern Alxa block, NW China: New constraints on the relationship between the North China Plate and the Alxa block. *Journal of Structural Geology*, 57: 38–57.

Zhang, J.J., and Zheng, Y.D., 1997. Polar Mohr constructions for strain analysis in general shear zones. *Journal of Structural Geology*, 19: 745–748.

Zhang, L., Wu, H., Wan, B., and Chen, Z., 2009a. Ages and geodynamic settings of Xilamulun Mo-Cu metallogenic belt in the northern part of the North China Craton. *Gondwana Research*, 16: 243–254.

Zhang, S.H., Zhao, Y., Liu, J.M., Hu, J.M., Song, B., Liu, J., and Wu, H., 2010. Geochronology, geochemistry and tectonic setting of the Late Paleozoice Early Mesozoic magmatism in the northern margin of the North China block: a preliminary review. *Acta Petrologica Sinica*, 29 (6): 824–842 (in Chinese with English abstract).

Zhang, S.H., Zhao, Y., Song, B., Hu, J.M., Liu, S.W., Yang, Y.H., Chen, F.K., Liu, X.M., and Liu, J., 2009b. Contrasting Late Carboniferous and Late Permian-Middle Triassic intrusive suites from the northern margin of the North China craton: geochronology, petrogenesis, and tectonic implications. *Geological Society Of America Bulletin*, 121: 181–200.

Zhang, S.H., Zhao, Y., Ye, H., Hou, K.J., and Li, C.F., 2012. Early Mesozoic alkaline complexes in the northern North China Craton: implications for cratonic lithospheric destruction. *Lithos*, 155: 1–18.

Zhang, X., Li, T., Pu, Z., and Wang, H., 2002. ^{40}Ar-^{39}Ar ages of the Louzidian-Dachengzi ductile shear zone near Chifeng, Inner Mongolia and their tectonic significance. *Chinese Science Bulletin*, 47: 1292–1297.

Zhang, X.H., and Zhai, M.G., 2010. Magmatism and its metallogenetic effects during the Paleozoic continental crustal construction in northern North China: an overview. *Acta Petrologica Sinica*, 26: 1329–1341(in Chinese with English abstract).

Zhao, P., Chen, Y., Xu, B., Faure, M., Shi, G., and Choulet, F., 2013. Did the Paleo-Asian Ocean between North China Block and Mongolia Block exist during the late Paleozoic? First paleomagnetic evidence from central-eastern Inner Mongolia, China. *Journal of Geophysical Research: Solid Earth*, 118: 1873–1894.

Zhao, P., Faure, M., Chen, Y., Shi, G., and Xu, B., 2015. A new Triassic shortening-extrusion tectonic model for Central-Eastern Asia: Structural, geochronological and paleomagnetic investigations in the Xilamulun Fault (North China). *Earth and Planetary Science Letters*, 426: 46–57.

Zheng, Y.D., 1999. Kinematic vorticity number and shear type related to the Yagan metamorphic core complex Sino-Mongolian border. *Scientia Geologica Sinica*, 34: 273–280 (in Chinese with English abstract).

Zheng, Y.D., and Chang, Z.Z., 1985. Finite Strain Measurement and Ductile Shear Zones. *Beijing: Geological Publishing House*, 35–102 (in Chinese).

Zheng, Y.D., and Wang, T., 2005. Kinematics and dynamics of the Mesozoic orogeny and late-orogenic extensional collapse in the Sino-Mongolian border areas. *Science in China (Earth Sciences)*, 48: 849–862.

Zheng, Y.D., Wang, T., and Wang, X.S., 2007. Theory and practice of the Maximum Effective Moment Criterion (MEMC). *Acta Scientiarum Naturalium Universitatis Pekinensis*, 43: 145–156 (in Chinese with English abstract).

Zhou, J.B., and Wilde, S.A., 2013. The crustal accretion history and tectonic evolution of the NE China segment of the Central Asian Orogenic Belt. *Gondwana Research*, 23: 1365–1377.

Zhou, J.B., Wilde, S. A., Zhao, G. C., and Han, J., 2018. Nature and assembly of microcontinental blocks within the Paleo-Asian Ocean. *Earth-Science Reviews*, 186: 76–93

Zhu, G., Xu, Y.D., Liu, G.S., Wang, Y.S., and Xie, C.L., 2006. Structural and deformational characteristics of strike-slippings along the middle-southern sector of the Tan-Lu faut zone. *Chinese Journal of Geology*, 41(2): 226–241 (in Chinese with English abstract).

Zorin, Y.A., 1999. Geodynamics of the western part of the Mongolia-Okhotsk collisional belt, Trans-Baikal region (Russia) and Mongolia. *Tectonophysics*, 306: 33–56.

About the first author

LIANG Chenyue, male, born in 1986 in Shuozhou City, Shanxi Province; doctor; graduated from University of Salzburg; lecturer of College of Earth Sciences, Jilin University. He is now interested in the study on rheology and deformation mechanism of natural rocks, microstructures, and tectono-thermochronology. Email: chenyueliang@jlu.edu.cn; phone: 15164362972.

About the corresponding author

LIU Yongjiang, male, born in 1964 in Mudanjiang City, Heilongjiang Province; doctor; graduated from University of Salzburg; research assistant of College of Marine Geosciences, Ocean University of China. He is now interested in the study on structural geology, and tectonics. Email: liuyongjiang@ouc.edu.cn; phone: 13844803058.